

UNIVERSIDAD POLITÉCNICA DE MADRID
ESCUELA TÉCNICA SUPERIOR DE INGENIEROS DE
TELECOMUNICACIÓN



TESIS DOCTORAL

A NEW ANALOG TRIGGER SYSTEM FOR THE CHERENKOV
TELESCOPE ARRAY

LUIS ÁNGEL TEJEDOR ÁLVAREZ

Ingeniero de Telecomunicación

2014

DEPARTAMENTO DE SEÑALES, SISTEMAS Y RADIOPROGRAMACIONES

ESCUELA TÉCNICA SUPERIOR DE INGENIEROS DE TELECOMUNICACIÓN

UNIVERSIDAD POLITÉCNICA DE MADRID

A NEW ANALOG TRIGGER SYSTEM FOR THE CHERENKOV
TELESCOPE ARRAY

TESIS DOCTORAL

Autor:

Luis Ángel Tejedor Álvarez
Ingeniero de Telecomunicación

Directores:

José Ignacio Alonso Montes
Catedrático del Departamento de Señales, Sistemas y Radiocomunicaciones
Universidad Politécnica de Madrid

Juan Abel Barrio Uña
Profesor Titular del Departamento de Física Atómica, Molecular y Nuclear
Universidad Complutense de Madrid

2014

TESIS DOCTORAL

A NEW ANALOG TRIGGER SYSTEM FOR THE CHERENKOV TELESCOPE ARRAY

AUTOR: Luis Ángel Tejedor Álvarez

DIRECTORES: José Ignacio Alonso Montes

Juan Abel Barrio Uña

PRESIDENTE:

SECRETARIO:

VOCAL:

VOCAL:

VOCAL:

SUPLENTE:

SUPLENTE:

Calificación:

EL PRESIDENTE

LOS VOCALES

EL SECRETARIO

Agradecimientos

Me siento tentado a rememorar en esta sección la mítica frase de Bart Simpson bendiciendo la mesa: “Como estos alimentos los hemos comprado nosotros, gracias por nada”. A fin de cuentas, yo he hecho la mayor parte del trabajo, yo he escrito los artículos publicados en revistas y yo he escrito esta tesis. Sin embargo, pensando un poco, me doy cuenta de que hay mucha más gente detrás que, si bien no han trabajado directamente en esta tesis, al menos han contribuido a crear las condiciones necesarias para que yo pudiera hacerla.

Para empezar, quiero dar las gracias a mis padres y a mi hermana. No sólo por su apoyo incondicional y demás reconocimientos morales (que también), sino porque, directamente, sé que si no hubiera vivido con ellos hasta los 30 nunca hubiera tenido tiempo material para terminar este doctorado. Así que realmente, esta tesis es en parte suya, por aguantarme estos años siempre liado delante del ordenador y sin tiempo para nada.

Otras dos personas fundamentales sin las que esta tesis no habría sido posible han sido mis dos directores de tesis, Juan Abel Barrio y José Ignacio Alonso. En este caso tengo que reconocer que, si la calidad tanto de la tesis como de los artículos publicados ha sido alta, se ha debido en buena parte a sus consejos y a lo que me han enseñado. La elaboración de esta tesis ha requerido unir conocimientos tanto del mundo de la ciencia como de la ingeniería, y ambos me han enseñado lo mejor de sus respectivos campos, a la vez que han hecho un gran esfuerzo por comprender lo del otro. Al final creo que los tres hemos aprendido mucho trabajando juntos.

A continuación quiero dar las gracias a todo el Grupo de Altas Energías (GAE) de la UCM, por haberme dado un sitio donde realizar un trabajo con el que disfruto y me siento realizado. Soy muy afortunado por poder dedicar mis esfuerzos a una causa tan bonita y apasionante como desentrañar los secretos del Universo. Dentro del grupo merecen una mención especial M^a Victoria Fonseca, por confiar en mí tras aquella primera entrevista en la que vio en mí “una gran energía”, y José Luis Contreras, que se deja la piel cada día por conseguir que España y el GAE tengamos un papel importante en CTA. Sin el trabajo de José Luis mi puesto de trabajo no habría existido y esta tesis no habría sido posible, así de claro.

Otras dos personas del GAE fundamentales en esta tesis han sido los dos compañeros de laboratorio con los que he tenido el privilegio de compartir muchas horas estos años: los ingenieros José Luis Lemus y Diego Herranz. Con ellos he aprendido a diseñar PCBs, a programar FPGAs y a usar LabView, hemos ido a La Palma, me han sustituido en reuniones, hemos diseñado juntos, hemos medido, hemos fracasado y hemos vuelto a diseñar, y así un día tras otro hasta conseguir hacer que las cosas funcionaran. Parte de esta tesis también es suya.

Tampoco quiero olvidarme de mis otros compañeros del GAE, tanto los que ya se fueron como los que aún siguen por aquí. No voy a mencionarlos personalmente de uno en uno porque son muchos, pero debo decir que me habéis hecho las comidas, los cafés, las reuniones que hemos organizado y mis primeras experiencias docentes sumamente agradables. Además, vuestros trabajos han sido las fuentes fundamentales para la elaboración del capítulo 2 de esta tesis.

Fuera del GAE también ha habido personas con importantes contribuciones a esta tesis: son los coautores de los artículos que, fundamentalmente desde el IFAE, el Ciemat y la UB han colaborado conmigo en el desarrollo del trigger. Voy a nombrar específicamente a Gustavo Martínez y a Juan Boix porque son los ingenieros con los que he trabajado más directamente durante todo el proyecto, pero ha habido muchas más personas de CTA España contribuyendo con desarrollos electrónicos,

mecánicos, simulaciones, o simplemente asistiendo a reuniones por todo el mundo donde presentar y defender nuestro trabajo.

A nivel internacional quiero dar las gracias a nuestros compañeros de los proyectos Dragon y NECTAr por contar con nosotros para las cámaras de los LSTs y MSTs, abrirnos las puertas de sus laboratorios, ayudarnos a hacer pruebas, compartir sus conocimientos y, en definitiva, por colaborar con nosotros para construir los mejores telescopios Cherenkov posibles.

Para terminar, quiero dar las gracias también a los proyectos FPA-2010-22056-C06-00, FPA2009-14226-C05-0, al CPAN (CSD2007-00042) y quizá también a otros proyectos de la Secretaría de Estado para la Investigación, Desarrollo e Innovación de los que desconozco sus códigos administrativos, por financiar el trabajo presentado. Gracias a los creadores de los proyectos, y a todos los contribuyentes que a través de sus impuestos hacen posibles proyectos como CTA.

En resumen, como esta tesis la hemos hecho entre todos, gracias por todo.

Resumen

La astronomía de rayos γ estudia las partículas más energéticas que llegan a la Tierra desde el espacio. Estos rayos γ no se generan mediante procesos térmicos en simples estrellas, sino mediante mecanismos de aceleración de partículas en objetos celestes como núcleos de galaxias activos, púlsares, supernovas, o posibles procesos de aniquilación de materia oscura. Los rayos γ procedentes de estos objetos y sus características proporcionan una valiosa información con la que los científicos tratan de comprender los procesos físicos que ocurren en ellos y desarrollar modelos teóricos que describan su funcionamiento con fidelidad.

El problema de observar rayos γ es que son absorbidos por las capas altas de la atmósfera y no llegan a la superficie (de lo contrario, la Tierra sería inhabitable). De este modo, sólo hay dos formas de observar rayos γ : embarcar detectores en satélites, u observar los efectos secundarios que los rayos γ producen en la atmósfera. Cuando un rayo γ llega a la atmósfera, interacciona con las partículas del aire y genera un par electrón - positrón, con mucha energía. Estas partículas secundarias generan a su vez más partículas secundarias cada vez menos energéticas. Estas partículas, mientras aún tienen energía suficiente para viajar más rápido que la velocidad de la luz en el aire, producen una radiación luminosa azulada conocida como radiación Cherenkov durante unos pocos nanosegundos.

Desde la superficie de la Tierra, algunos telescopios especiales, conocidos como telescopios Cherenkov o IACTs (Imaging Atmospheric Cherenkov Telescopes), son capaces de detectar la radiación Cherenkov e incluso de tomar imágenes de la forma de la cascada Cherenkov. A partir de estas imágenes es posible conocer las principales características del rayo γ original, y con suficientes rayos γ se pueden deducir características importantes del objeto que los emitió, a cientos de años luz de distancia.

Sin embargo, detectar cascadas Cherenkov procedentes de rayos γ no es nada fácil. Las cascadas generadas por fotones γ de bajas energías emiten pocos fotones, y durante pocos nanosegundos, y las correspondientes a rayos γ de alta energía, si bien producen más electrones y duran más, son más improbables conforme mayor es su energía. Esto produce dos líneas de desarrollo de telescopios Cherenkov: Para observar cascadas de bajas energías son necesarios grandes reflectores que recuperen muchos fotones de los pocos que tienen estas cascadas. Por el contrario, las cascadas de altas energías se pueden detectar con telescopios pequeños, pero conviene cubrir con ellos una superficie grande en el suelo para aumentar el número de eventos detectados.

Con el objetivo de mejorar la sensibilidad de los telescopios Cherenkov actuales, en el rango de energía alto (> 10 TeV), medio (100 GeV - 10 TeV) y bajo (10 GeV - 100 GeV), nació el proyecto CTA (Cherenkov Telescope Array). Este proyecto en el que participan más de 27 países, pretende construir un observatorio en cada hemisferio, cada uno de los cuales contará con 4 telescopios grandes (LSTs), unos 30 medianos (MSTs) y hasta 70 pequeños (SSTs). Con un array así, se conseguirán dos objetivos. En primer lugar, al aumentar drásticamente el área de colección respecto a los IACTs actuales, se detectarán más rayos γ , en todos los rangos de energía. En segundo lugar, cuando una misma cascada Cherenkov es observada por varios telescopios a la vez, es posible analizarla con mucha más precisión gracias a las técnicas estereoscópicas.

La presente tesis recoge varios desarrollos técnicos realizados como aportación a los telescopios medianos y grandes de CTA, concretamente al sistema de trigger. Al ser las cascadas Cherenkov tan breves, los sistemas que digitalizan y leen los datos de cada píxel tienen que funcionar a frecuencias muy altas (≈ 1 GHz), lo que hace inviable que funcionen de forma continua, ya que la cantidad de

datos guardada sería inmanejable. En su lugar, las señales analógicas se muestran, guardando las muestras analógicas en un buffer circular de unos pocos μ s. Mientras las señales se mantienen en el buffer, el sistema de trigger hace un análisis rápido de las señales recibidas, y decide si la imagen que hay en el buffer corresponde a una cascada Cherenkov y merece ser guardada, o por el contrario puede ignorarse permitiendo que el buffer se sobreescriba.

La decisión de si la imagen merece ser guardada o no, se basa en que las cascadas Cherenkov producen detecciones de fotones en píxeles cercanos y en tiempos muy próximos, a diferencia de los fotones de NSB (night sky background), que llegan aleatoriamente. Para detectar cascadas grandes es suficiente con comprobar que más de un cierto número de píxeles en una región hayan detectado más de un cierto número de fotones en una ventana de tiempo de algunos nanosegundos. Sin embargo, para detectar cascadas pequeñas es más conveniente tener en cuenta cuántos fotones han sido detectados en cada píxel (técnica conocida como *sumtrigger*). El sistema de trigger desarrollado en esta tesis pretende optimizar la sensibilidad a bajas energías, por lo que suma analógicamente las señales recibidas en cada píxel en una región de trigger y compara el resultado con un umbral directamente expresable en fotones detectados (photoelectrones). El sistema diseñado permite utilizar regiones de trigger de tamaño seleccionable entre 14, 21 o 28 píxeles (2, 3, o 4 clusters de 7 píxeles cada uno), y con un alto grado de solapamiento entre ellas. De este modo, cualquier exceso de luz en una región compacta de 14, 21 o 28 píxeles es detectado y genera un pulso de trigger. En la versión más básica del sistema de trigger, este pulso se distribuye por toda la cámara de forma que todos los clusters sean leídos al mismo tiempo, independientemente de su posición en la cámara, a través de un delicado sistema de distribución.

De este modo, el sistema de trigger guarda una imagen completa de la cámara cada vez que se supera el número de fotones establecido como umbral en una región de trigger. Sin embargo, esta forma de operar tiene dos inconvenientes principales. En primer lugar, la cascada casi siempre ocupa sólo una pequeña zona de la cámara, por lo que se guardan muchos píxeles sin información alguna. Cuando se tienen muchos telescopios como será el caso de CTA, la cantidad de información inútil almacenada por este motivo puede ser muy considerable. Por otro lado, cada trigger supone guardar unos pocos nanosegundos alrededor del instante de disparo. Sin embargo, en el caso de cascadas grandes la duración de las mismas puede ser bastante mayor, perdiéndose parte de la información debido al truncamiento temporal. Para resolver ambos problemas se ha propuesto un esquema de trigger y lectura basado en dos umbrales. El umbral alto decide si hay un evento en la cámara y, en caso positivo, sólo las regiones de trigger que superan el nivel bajo son leídas, durante un tiempo más largo. De este modo se evita guardar información de píxeles vacíos y las imágenes fijas de las cascadas se pueden convertir en pequeños “vídeos” que representen el desarrollo temporal de la cascada. Este nuevo esquema recibe el nombre de COLIBRI (Concept for an Optimized Local Image Building and Readout Infrastructure), y se ha descrito detalladamente en el capítulo 5.

Un problema importante que afecta a los esquemas de sumtrigger como el que se presenta en esta tesis es que para sumar adecuadamente las señales provenientes de cada píxel, estas deben tardar lo mismo en llegar al sumador. Los fotomultiplicadores utilizados en cada píxel introducen diferentes retardos que deben compensarse para realizar las sumas adecuadamente. El efecto de estos retardos ha sido estudiado, y se ha desarrollado un sistema para compensarlos.

Por último, el siguiente nivel de los sistemas de trigger para distinguir efectivamente las cascadas Cherenkov del NSB consiste en buscar triggers simultáneos (o en tiempos muy próximos) en telescopios vecinos. Con esta función, junto con otras de interfaz entre sistemas, se ha desarrollado un sistema denominado Trigger Interface Board (TIB). Este sistema consta de un módulo que

irá montado en la cámara de cada LST o MST, y que estará conectado mediante fibras ópticas a los telescopios vecinos. Cuando un telescopio tiene un trigger local, este se envía a todos los vecinos conectados y viceversa, de modo que cada telescopio sabe si sus vecinos han dado trigger. Una vez compensadas las diferencias de retardo debidas a la propagación en las fibras ópticas y de los propios fotones Cherenkov en el aire dependiendo de la dirección de apuntamiento, se buscan coincidencias, y en el caso de que la condición de trigger se cumpla, se lee la cámara en cuestión, de forma sincronizada con el trigger local.

Aunque todo el sistema de trigger es fruto de la colaboración entre varios grupos, fundamentalmente IFAE, CIEMAT, ICC-UB y UCM en España, con la ayuda de grupos franceses y japoneses, el núcleo de esta tesis son el Level 1 y la Trigger Interface Board, que son los dos sistemas en los que el autor ha sido el ingeniero principal. Por este motivo, en la presente tesis se ha incluido abundante información técnica relativa a estos sistemas. Existen actualmente importantes líneas de desarrollo futuras relativas tanto al trigger de la cámara (implementación en ASICs), como al trigger entre telescopios (trigger topológico), que darán lugar a interesantes mejoras sobre los diseños actuales durante los próximos años, y que con suerte serán de provecho para toda la comunidad científica participante en CTA.

Abstract

γ -ray astronomy studies the most energetic particles arriving to the Earth from outer space. These γ -rays are not generated by thermal processes in mere stars, but by means of particle acceleration mechanisms in astronomical objects such as active galactic nuclei, pulsars, supernovas or as a result of dark matter annihilation processes. The γ -rays coming from these objects and their characteristics provide valuable information to the scientist which try to understand the underlying physical fundamentals of these objects, as well as to develop theoretical models able to describe them accurately.

The problem when observing γ rays is that they are absorbed in the highest layers of the atmosphere, so they don't reach the Earth surface (otherwise the planet would be uninhabitable). Therefore, there are only two possible ways to observe γ -rays: by using detectors on-board of satellites, or by observing their secondary effects in the atmosphere. When a γ -ray reaches the atmosphere, it interacts with the particles in the air generating a highly energetic electron-positron pair. These secondary particles generate in turn more particles, with less energy each time. While these particles are still energetic enough to travel faster than the speed of light in the air, they produce a bluish radiation known as Cherenkov light during a few nanoseconds.

From the Earth surface, some special telescopes known as Cherenkov telescopes or IACTs (Imaging Atmospheric Cherenkov Telescopes), are able to detect the Cherenkov light and even to take images of the Cherenkov showers. From these images it is possible to know the main parameters of the original γ -ray, and with some γ -rays it is possible to deduce important characteristics of the emitting object, hundreds of light-years away.

However, detecting Cherenkov showers generated by γ -rays is not a simple task. The showers generated by low energy γ -rays contain few photons and last few nanoseconds, while the ones corresponding to high energy γ -rays, having more photons and lasting more time, are much more unlikely. This results in two clearly differentiated development lines for IACTs: In order to detect low energy showers, big reflectors are required to collect as much photons as possible from the few ones that these showers have. On the contrary, small telescopes are able to detect high energy showers, but a large area in the ground should be covered to increase the number of detected events.

With the aim to improve the sensitivity of current Cherenkov showers in the high (> 10 TeV), medium (100 GeV - 10 TeV) and low (10 GeV - 100 GeV) energy ranges, the CTA (Cherenkov Telescope Array) project was created. This project, with more than 27 participating countries, intends to build an observatory in each hemisphere, each one equipped with 4 large size telescopes (LSTs), around 30 middle size telescopes (MSTs) and up to 70 small size telescopes (SSTs). With such an array, two targets would be achieved. First, the drastic increment in the collection area with respect to current IACTs will lead to detect more γ -rays in all the energy ranges. Secondly, when a Cherenkov shower is observed by several telescopes at the same time, it is possible to analyze it much more accurately thanks to the stereoscopic techniques.

The present thesis gathers several technical developments for the trigger system of the medium and large size telescopes of CTA. As the Cherenkov showers are so short, the digitization and readout systems corresponding to each pixel must work at very high frequencies (≈ 1 GHz). This makes unfeasible to read data continuously, because the amount of data would be unmanageable. Instead, the analog signals are sampled, storing the analog samples in a temporal ring buffer able to store up to a few μ s. While the signals remain in the buffer, the trigger system performs a fast analysis of

the signals and decides if the image in the buffer corresponds to a Cherenkov shower and deserves to be stored, or on the contrary it can be ignored allowing the buffer to be overwritten.

The decision of saving the image or not, is based on the fact that Cherenkov showers produce photon detections in close pixels during near times, in contrast to the random arrival of the NSB phtotons. Checking if more than a certain number of pixels in a trigger region have detected more than a certain number of photons during a certain time window is enough to detect large showers. However, taking also into account how many photons have been detected in each pixel (sumtrigger technique) is more convenient to optimize the sensitivity to low energy showers. The developed trigger system presented in this thesis intends to optimize the sensitivity to low energy showers, so it performs the analog addition of the signals received in each pixel in the trigger region and compares the sum with a threshold which can be directly expressed as a number of detected photons (photoelectrons). The trigger system allows to select trigger regions of 14, 21, or 28 pixels (2, 3 or 4 clusters with 7 pixels each), and with extensive overlapping. In this way, every light increment inside a compact region of 14, 21 or 28 pixels is detected, and a trigger pulse is generated. In the most basic version of the trigger system, this pulse is just distributed throughout the camera in such a way that all the clusters are read at the same time, independently from their position in the camera, by means of a complex distribution system.

Thus, the readout saves a complete camera image whenever the number of photoelectrons set as threshold is exceeded in a trigger region. However, this way of operating has two important drawbacks. First, the shower usually covers only a little part of the camera, so many pixels without relevant information are stored. When there are many telescopes as will be the case of CTA, the amount of useless stored information can be very high. On the other hand, with every trigger only some nanoseconds of information around the trigger time are stored. In the case of large showers, the duration of the shower can be quite larger, loosing information due to the temporal cut. With the aim to solve both limitations, a trigger and readout scheme based on two thresholds has been proposed. The high threshold decides if there is a relevant event in the camera, and in the positive case, only the trigger regions exceeding the low threshold are read, during a longer time. In this way, the information from empty pixels is not stored and the fixed images of the showers become to little “videos” containing the temporal development of the shower. This new scheme is named COLIBRI (Concept for an Optimized Local Image Building and Readout Infrastructure), and it has been described in depth in chapter 5.

An important problem affecting sumtrigger schemes like the one presented in this thesis is that in order to add the signals from each pixel properly, they must arrive at the same time. The photomultipliers used in each pixel introduce different delays which must be compensated to perform the additions properly. The effect of these delays has been analyzed, and a delay compensation system has been developed.

The next trigger level consists of looking for simultaneous (or very near in time) triggers in neighbour telescopes. These function, together with others relating to interfacing different systems, have been developed in a system named Trigger Interface Board (TIB). This system is comprised of one module which will be placed inside the LSTs and MSTs cameras, and which will be connected to the neighbour telescopes through optical fibers. When a telescope receives a local trigger, it is resent to all the connected neighbours and vice-versa, so every telescope knows if its neighbours have been triggered. Once compensated the delay differences due to propagation in the optical fibers and in the air depending on the pointing direction, the TIB looks for coincidences, and in the case that the trigger condition is accomplished, the camera is read a fixed time after the local trigger arrived.

Despite all the trigger system is the result of the cooperation of several groups, specially IFAE, Ciemat, ICC-UB and UCM in Spain, with some help from french and japanese groups, the Level 1 and the Trigger Interface Board constitute the core of this thesis, as they have been the two systems designed by the author of the thesis. For this reason, a large amount of technical information about these systems has been included. There are important future development lines regarding both the camera trigger (implementation in ASICS) and the stereo trigger (topological trigger), which will produce interesting improvements for the current designs during the following years, being useful for all the scientific community participating in CTA.

Author publications

The work presented in this thesis has given rise to several publications and conference papers.

Publications of the author

1. L.A. Tejedor, M. Barceló, J. Boix, G. Martínez, J.A. Barrio, O. Blanch and C. Delgado
An Analog Trigger System for Atmospheric Cherenkov Telescope Arrays.
IEEE Transactions on Nuclear Science, vol. 60, issue 3, pp. 2367-2375, May. 2013.
doi:10.1109/TNS.2013.2257852
2. M. Barceló, J.A. Barrio, O. Blanch Bigas, J. Boix, C. Delgado, D. Herranz, R. López-Coto, G. Martínez, L.A. Tejedor, for the CTA Consortium
An Analog Trigger System for Atmospheric Cherenkov Telescopes
Proc of the 33rd Int. Cosmic Ray Conference, Rio de Janeiro, Brazil, 2013.
arXiv:1307.3169 [astro-ph.IM]
3. L. A. Tejedor, J. I. Alonso, J. A. Barrio, J. L. Lemus and C. Delgado
An Analog Level 1 Trigger Prototype for CTA.
IEEE Transactions on Nuclear Science, vol. 60, no. 1, pp. 251-258, Feb. 2013
doi:10.1109/TNS.2012.2226246
4. L.A. Tejedor, J.I. Alonso and J.A. Barrio
Divisores Wilkinson con Elementos Concentrados para Procesado de Pulses
26th Nat. Symp. of the URSI, Leganés, Spain, Sept. 2011
http://www.gae.ucm.es/~ltejedor/divisores_concentrados_pulsos.pdf
5. L.A. Tejedor
Puerta Lógica Diferencial de N Entradas
Spanish Patent. Publication Number ES2392085 A1, Dec. 2012
http://www.oepm.es/pdf/ES/0000/000/02/39/20/ES-2392085_A1.pdf
6. C.L. Naumann, L.A. Tejedor and G. Martínez
COLIBRI: partial camera readout and sliding trigger for the Cherenkov Telescope Array CTA
Journal of Instrumentation, vol.8, P06011 Jun. 2013
doi:10.1088/1748-0221/8/06/P06011
7. L.A. Tejedor, J. Boix, F. Dubois, Y. Konno, D. Herranz, J.A. Barrio and J.I. Alonso
An analog delay compensation system to reduce the effect of variable transit time in PMTs
IEEE Transactions on Nuclear Science, vol. 60, issue 4, pp. 2905-2911, Aug. 2013
doi:10.1109/TNS.2013.2271300

Publications of the author, as a member of the CTA Consortium

1. B.S. Acharya, L.A. Tejedor, et al, for the CTA Consortium
Introducing the CTA concept
Astroparticle Physics, vol. 43, pp. 3-18, March 2013
doi:10.1016/j.astropartphys.2013.01.007
2. The CTA Consortium.
Design Concepts for the Cherenkov Telescope Array CTA: an advanced facility for ground-based high-energy gamma-ray astronomy
Experimental Astronomy, vol.32, issue 3, pp. 193-316, Dec. 2011
doi:10.1007/s10686-011-9247-0
3. G. Ambrosi, Y. Awane, H. Baba, A. Bamba, M. Barceló, U. Barres de Almeida, J.A. Barrio, O. Blanch-Bigas, J. Boix, L. Brunetti, E. Carmona, E. Chabanne, M. Chikawa, P. Colin, J.L. Contreras, J. Cortina, F. Dazzi, A. Deangelis, G. Deeglise, C. Delgado, C. Díaz, F. Dubois, A. Fiasson, D. Fink, N. Fouque, L. Freixas, C. Fruck, A. Gadola, R. García, D. Gascón, N. Gefroy, N. Giglietto, F. Giordano, F. Grañena, S. Gunji, R. Hagiwara, N. Hamer, Y. Hanabata, T. Hassan, K. Hatanaka, T. Haubold, M. Hayashida, R. Hermel, D. Herranz, K. Hirotani, S. Inoue, Y. Inoue, K. Ioka, C. Jablonski, M. Kagaya, H. Katagiri, T. Kishimoto, K. Kodani, K. Kohri, Y. Konno, S. Koyama, H. Kubo, J. Kushida, G. Lamanna, T. Le Flour, M. López-Moya, R. López, E. Lorenz, P. Majumdar, A. Manalaysay, M. Mariotti, G. Martínez, M. Martínez, D. Mazin, J.M. Miranda, R. Mirzoyan, I. Monteiro, A. Moralejo, K. Murase, S. Nagataki, D. Nakajima, T. Nakamori, K. Nishijima, K. Noda, A. Nozato, Y. Ohira, M. Ohishi, H. Ohoka, A. Okumura, R. Orito, J.L. Panazol, D. Paneque, R. Paoletti, J.M. Paredes, G. Pauletta, S. Podkladkin, J. Prast, R. Rando, O. Reimann, M. Ribó, S. Rosier-Less, K. Saito, T. Saito, Y. Saito, N. Sakaki, R. Sakonaka, A. Sanuy, H. Sasaki, M. Sawada, V. Scalzotto, S. Schultz, T. Schweizer, T. Shibata, S. Shu, J. Sieiro, V. Stamatescu, S. Steiner, U. Straumann, R. Sugawara, H. Tajima, H. Takami, S. Tanaka, L.A. Tejedor, Y. Terada, M. Teshima, T. Totani, H. Ueno, K. Umehara, A. Vollhardt, R. Wagner, H. Wetteskind, T. Yamamoto, R. Yamazaki, A. Yoshida, T. Yoshikoshi, for the CTA Consortium.
The Cherenkov Telescope Array Large Size Telescope
Proc of the 33rd Int. Cosmic Ray Conference, Rio de Janeiro, Brazil, 2013.
arXiv:1307.4565 [astro-ph.IM]
4. J.F. Glicenstein, M. Barceló, J.A. Barrio, O. Blanch, J. Boix, J. Bolmont, C. Boutonnet, S. Cazaux, E. Chabanne, C. Champion, F. Chateau, S. Colonges, P. Corona, S. Couturier, B. Courty, E. Delagnes, C. Delgado, J.P. Ernenwein, S. Fegan, O. Ferreira, M. Fesquet, G. Fontaine, N. Fouque, F. Henault, D. Gascón, D. Herranz, R. Hermel, D. Hoffmann, J. Houles, S. Karkar, B. Khelifi, J. Knöldlseder, G. Martínez, K. Lacombe, G. Lamanna, T. LeFlour, R. López-Coto, F. Louis, A. Mathieu, E. Moulin, P. Nayman, F. Nunio, J.F. Olive, J.L. Panazol, P.O. Petrucci, M. Punch, J. Prast, P. Ramon, M. Riallot, M. Ribó, S. Rosier-Less, A. Sanuy, J. Sieiro, J.P. Tavernet, L.A. Tejedor, F. Toussenel, G. Vasileiadis, V. Voisin, V. Waegebert, C. Zurbach, for the CTA Consortium.

The NectarCAM camera project

Proc of the 33rd Int. Cosmic Ray Conference, Rio de Janeiro, Brazil, 2013.

arXiv:1307.4545 [astro-ph.IM]

5. H. Kubo, R. Paoletti, Y. Awane, A. Bamba, M. Barceló, J.A. Barrio, O. Blanch, J. Boix, C. Delgado, D. Fink, D. Gascón, S. Gunji, R. Hagiwara, Y. Hanabata, K. Hatanaka, M. Hayashida, M. Ikeno, S. Kabuki, H. Katagiri, J. Kataoka, Y. Konno, S. Koyama, T. Kishimoto, J. Kushida, G. Martínez, S. Masuda, J.M. Miranda, R. Mirzoyan, T. Mizuno, T. Nagayoshi, D. Nakajima, T. Nakamori, H. Ohoka, A. Okumura, R. Orito, T. Saito, A. Sanuy, H. Sasaki, M. Sawada, T. Schweizer, R. Sugawara, K.H. Sulanke, H. Tajima, M. Tanaka, S. Tanaka, L.A. Tejedor, Y. Terada, M. Teshima, F. Tokanai, Y. Tsuchiya, T. Uchida, H. Ueno, K. Umehara, T. Yamamoto, for the CTA Consortium.

Development of the Photomultiplier-Tube Readout System for the CTA Large Size Telescope

Proc of the 33rd Int. Cosmic Ray Conference, Rio de Janeiro, Brazil, 2013.

arXiv:1307.3386 [astro-ph.IM]

6. J.F. Glicenstein, et al.

Status of the NectarCAM camera project

Proc. of the 2014 SPIE Astronomical Telescopes + Instrumentation, Quebec, Canada, 2014.

Contents

1	Introduction.	1
2	Ground based gamma-ray astronomy and Cherenkov telescopes	3
2.1	Gamma-ray astronomy	3
2.2	Gamma-ray detection techniques	7
2.2.1	Direct detection by on-board satellite detectors	8
2.2.2	Ground-based detectors: the Cherenkov technique	8
2.2.3	Sensitivity of an IACT	11
2.2.3.1	Integral sensitivity	13
2.2.3.2	Differential sensitivity	13
2.2.3.3	Effective collection area	14
2.2.4	Arrays of IACTs	15
2.2.5	Comparison between direct detection and Cherenkov technique	16
2.3	Imaging Atmospheric Cherenkov Telescopes	17
2.3.1	Mechanics	17
2.3.2	Optics	19
2.3.3	Photodetectors	20
2.3.3.1	Photomultipliers	21
2.3.3.2	Avalanche Photodiodes	22
2.3.3.3	Silicon Photomultipliers	22
2.3.3.4	Hybrid Photodetectors	24
2.3.3.5	Photodetector comparison	25
2.3.4	Readout systems	25
2.3.5	Data management	28
2.3.6	Auxiliary systems	28

2.3.6.1	Timing	28
2.3.6.2	Pointing	29
2.3.6.3	Calibration	29
2.3.6.4	Cooling	30
2.3.6.5	Weather conditions and security	30
2.4	The Cherenkov Telescope Array	30
2.4.1	Small Sized Telescopes	31
2.4.2	Medium Sized Telescopes	32
2.4.3	Large Sized Telescopes	32
2.4.4	Expected Sensitivity	33
3	The Trigger System.	37
3.1	Multi-level trigger basis	38
3.1.1	Pixel level	39
3.1.2	Camera level	39
3.1.2.1	Trigger-region based camera triggers	39
3.1.2.1.1	Majority	39
3.1.2.1.2	Sumtrigger	39
3.1.2.2	Pattern-recognition based camera triggers	41
3.1.3	Array level	43
3.2	An Analog Trigger System for CTA LSTs and MSTs	44
3.2.1	Camera hardware architecture	46
3.2.1.1	Pixel electronics	46
3.2.1.2	Front-end boards	47
3.2.1.3	Slow Control boards	49
3.2.1.4	Backplanes	49
3.2.1.5	Trigger interface board	50
3.2.1.6	Array trigger and clock board	51
3.2.1.7	Calibration box	51
3.2.1.8	Camera Slow Control System	51
3.2.2	Trigger architecture	52
3.2.3	Level 0	54
3.2.3.1	Majority	54
3.2.3.2	Sum	56

3.2.4	Level 0 fan-out	57
3.2.5	Level 1	60
3.2.6	Level 1 distribution	62
3.2.7	Performance of the trigger system at camera level	64
3.2.7.1	Latency and Jitter	65
3.2.7.2	Gain measurements with rate scans	67
3.2.7.3	Noise	68
3.2.7.4	Attenuation and clipping	69
3.2.7.5	Dynamic range	70
3.2.7.6	Pulse width	71
3.2.7.7	Power consumption	72
3.2.7.8	Summary of camera trigger parameters	72
3.2.8	Array trigger	73
3.2.8.1	LST hardware stereo trigger	73
3.2.8.2	Software array trigger	74
4	The Level 1	77
4.1	General scheme	78
4.2	Differential to single-ended converter	79
4.3	Wilkinson splitters	80
4.4	Attenuators	83
4.5	Switching network	83
4.6	Adders	84
4.7	Comparators	87
4.8	Digital to Analog Converter	87
4.9	OR Gate	89
4.9.1	Basic principles	90
4.9.2	Generic Gates	91
4.9.3	Transition Times	91
4.9.4	First gate prototypes	94
4.9.5	Level 1 OR Gate	96
4.10	Other technological issues	98
4.10.1	Dimensions	98
4.10.2	Connectors	98

4.10.3	PCB stack-up and routing	101
4.11	Test bench	101
4.12	Measurements	104
4.12.1	Gain and linearity	104
4.12.2	Noise	105
4.12.3	Pulse width and bandwidth	105
4.12.4	Latency	107
4.12.5	Time walk	109
4.12.6	Jitter	110
4.13	Level 1 conclusions	110
5	COLIBRI	113
5.1	Partial readout	113
5.2	Sliding readout window	114
5.3	Localized triggering and readout with a single threshold	116
5.4	Two-threshold trigger and readout	117
5.4.1	Timing considerations	117
5.5	Expected performance	119
5.5.1	Comparison between different readout schemes	120
5.5.2	Quality of reconstructed images	122
5.5.3	Gamma-hadron separation	123
5.6	Hardware implementation	124
5.6.1	Changes in the Level 1	124
5.6.2	Changes in the Level 1 distribution	125
5.7	Summary and suitability of COLIBRI	127
6	PMT Transit Time Compensation	129
6.1	Impact of the different transit times	129
6.2	Delay compensation with a reference	131
6.2.1	Delay lines	133
6.2.2	Delay meter	135
6.2.2.1	AND gate	136
6.2.2.2	Width to amplitude converter	137
6.2.2.3	Sample, hold and ADC reading	139

6.2.2.4	Power saving	141
6.3	Delay compensation without a reference	141
6.4	Conclusions about the transit time delay compensation	143
7	Trigger Interface Board.	145
7.1	Interfacing	146
7.1.1	Trigger types	149
7.1.2	Time stamp and event building	150
7.1.3	Pin definitions	150
7.2	Hardware stereo trigger	151
7.2.1	Timing restrictions	151
7.2.1.1	Compensation of the fixed delays	152
7.2.1.2	Compensation of the Cherenkov light time of flight	152
7.2.1.3	Synchronization with local trigger	155
7.3	Advanced features	156
7.3.1	More LSTs	158
7.3.2	MSTs contributing to the LST stereo trigger	159
7.3.3	Slow controllable functionalities	159
7.3.4	Busy state	160
7.3.5	Topologic stereo trigger	160
7.4	Technical description	161
7.4.1	General architecture	161
7.4.2	Optical links	161
7.4.2.1	Optical fibers	162
7.4.2.2	Transceivers	162
7.4.2.2.1	SFP modules	163
7.4.2.2.2	Discrete VCSELs and PiN photodiodes	164
7.4.3	External delays	166
7.4.4	FPGA and firmware	166
7.4.4.1	High level architecture	167
7.4.4.2	Programmable delay lines	169
7.4.4.3	Stretchers	170
7.4.4.4	Stereo Logic	171
7.4.4.5	Collector	173

7.4.4.6	ITR counters	174
7.4.4.7	SFP control	175
7.4.4.8	External delay control	175
7.4.4.9	Thermometer	176
7.4.4.10	Slow control module	176
7.4.5	Raspberry Pi	177
7.4.5.1	Interface with the FPGA	178
7.4.5.2	FPGA initialization	179
7.4.5.3	Interface with the slow control unit	179
7.4.5.4	Other functions in the Raspberry Pi	180
7.4.6	Power supply	181
7.4.7	Temperature monitoring	183
7.4.8	TIB PCB design	183
7.5	TIB measurements	186
7.5.1	Power supplies	186
7.5.2	FPGA configuration	187
7.5.3	Clock generation in the PLLs	187
7.5.4	FPGA delay lines	188
7.5.5	Stretchers	189
7.5.6	Stereo Logic	191
7.5.7	Collector	194
7.5.8	ITR counters	194
7.5.9	Optical links	194
7.5.10	External delays	196
7.5.10.1	Delays with DS1123LE-200	196
7.5.10.2	Delays with 3D3428	197
7.5.10.3	Delay with an optical fiber reel	198
7.5.11	Test conclusions	198

8 Conclusion and Outlook	201
8.1 Conclusions	201
8.2 Outlook	202
8.2.1 Trigger integration in ASICs	202
8.2.2 Topologic stereo trigger	203
8.2.2.1 Sectorization	205
8.2.2.2 Triangulation	206
A Schematics	209
A.1 Level 1 schematics	209
A.2 Trigger Interface Board schematics	223
B Bill of materials	237
B.1 Bill of materials of Level 1	237
B.2 Bill of materials of trigger interface board	240
C Reliability	243
Bibliography	249

List of Figures

2.1	X-ray, optical and infrared composite of Kepler's supernova remnant	4
2.2	Schematic and observation of a pulsar	5
2.3	Scheme and observation of an AGN	5
2.4	X-ray binary, artist impression	6
2.5	Image of GRB 080319B in X-ray (left) and optical (right)	6
2.6	First detections of ionization radiation in the atmosphere	7
2.7	History of gamma-ray astronomy by direct detection.	9
2.8	Extended Air Showers generated by γ -rays and cosmic-rays	10
2.9	Schematic simplification of the Cherenkov effect	10
2.10	Basic scheme of Cherenkov technique [20].	11
2.11	Images recorded by the camera of MAGIC-I telescope, corresponding to a γ -ray and a shower originated by an hadron	12
2.12	Integral sensitivity of the MAGIC stereo system. Black solid line represents the measured sensitivity, black dashed line the expected sensitivity from the MonteCarlo simulations, and grey line represents MAGIC-I integral sensitivity when working alone [21]. The flux is expressed in photons $\cdot cm^{-2} \cdot s^{-1}$	14
2.13	Differential sensitivity of the MAGIC stereo system , expressed in TeV $\cdot cm^{-2} \cdot s^{-1}$. Black points represent the differential sensitivity, black dashed line represents the differential sensitivity expected from the simulations, and the horizontal error bars represent the size of the bins in estimated energy [21]	14
2.14	Scheme of stereoscopic observation with an array of IACTs	15
2.15	Currently active arrays of IACTs	16
2.16	Relative particle flux vs energy. A similar behaviour can be observed for hadrons, muons and γ -rays	17
2.17	Comparison of integral sensitivities for ground based and satellite γ -ray experiments. The sensitivity is defined as the minimum flux of particles per square centimetre and second required to detect a source with a 5σ significance over the background after 50 hours observation for IACTs and 1 month for satellites [1],[26].	18

2.18	Some currently active Cherenkov telescopes	19
2.19	Scheme of one of the HESS mirror actuators [39]	19
2.20	Different optical schemes suitable for IACTs	20
2.21	Winston cones	21
2.22	Photomultipliers	22
2.23	APD scheme	23
2.24	Silicon Photomultipliers	23
2.25	Output pulse produced by a PMT (green) and a SiPM (yellow) [49]	24
2.26	Hybrid photodetector	25
2.27	Scheme of a readout based on analog memories	26
2.28	DRS4 and NECTAr chips	27
2.29	Rubidium clock synchronized by GPS, model Symmetricom XLI, like the one used in MAGIC	28
2.30	MAGIC mirror pointing calibration	29
2.31	CTA concept	31
2.32	Contries participating in the CTA Consortium	31
2.33	Some design concepts for the SSTs	32
2.34	Design concept for the MSTs	33
2.35	Design concept for the LSTs	33
2.36	Different possible array layouts. According to simulations, the most balanced performance is achieved by array E.	34
2.37	CTA expected performance for array E [2].	35
3.1	Recorded images for different kinds of events and NSB [10], [11]. The different colors indicate the amount of light collected by the pixels.	37
3.2	Level 1 MAGIC trigger regions [85]. In the figure only the inner pixels are shown, because the external ones do not participate in the original trigger scheme	40
3.3	Generic schemes of the majority and sum trigger	41
3.4	Collection area of the MAGIC-1 telescope with standard next-neighbour majority trigger (black dots) and sum trigger (grey dots)[86]	42
3.5	Trigger rate versus discriminator threshold of a MAGIC-I sum trigger region with clipping (black crosses and dark grey dots) and without it (light grey dots). The black crosses and the light grey dots represent rates obtained by means of Montecarlo simulations, while the dark grey dots correspond to rate measurements. For thresholds lower than 21 phe the NSB dominates, while for very high thresholds the rate is dominated by the cosmic-rays. In the middle thresholds is where the clipping effect is crucial.	42

3.6	Scheme of the HESS array trigger [83]	43
3.7	Simulated collection areas for different trigger schemes in CTA LSTs [93]	45
3.8	Simulated collection areas for different trigger schemes in CTA MSTs [93]	46
3.9	PMT and its associated electronics for LST	47
3.10	Dragon and NECTAr front-end boards	48
3.11	Slow control board	49
3.12	Backplane board	50
3.13	Trigger interface board	50
3.14	Photo of the calibration box used in MAGIC. The CTA one was not ready at the end of this thesis	52
3.15	Trigger architecture	53
3.16	Cluster with all the elements connected	53
3.17	Level 0 majority scheme	54
3.18	Some Level 0 circuit schemes	55
3.19	Photograph of the Level 0 Majority	56
3.20	Level 0 sum scheme	56
3.21	Level 0 attenuator circuit schematic	57
3.22	Photograph of the Level 0 Sum	57
3.23	Level 0 fan-out schematics	58
3.24	Photographs of the Level 0 fan-out backplane mezzanine	59
3.25	Measured voltage gain for different input amplitudes in the 6 output branches of the Level 0 fan-out module	60
3.26	Level 1 working modes	61
3.27	Level 1 mezzanine, version 3, in real scale	62
3.28	Level 1 distribution connection among neighbour clusters (left) and example of Level 1 distribution paths in the camera (right)	63
3.29	Level 1 distribution block diagram and circuit implementation	64
3.30	Level 1 distribution test bench	64
3.31	Level 1 distribution measurements	65
3.32	Two test benches for integrated tests of trigger subsystems and front-end boards	65
3.33	Global trigger latency [3]	66
3.34	Rate scan changing Level 1 threshold when only one pixel in cluster 0 is fired, with Level 0 majority	67
3.35	Rate scans corresponding to different additions of pixels and clusters	68

3.36 Rate scan for input amplitudes corresponding to 8, 4, 2, 1 phe and only noise, when the Level 1 is working in mode 4	69
3.37 Rate scans changing the attenuation or the clipping control voltages	69
3.38 Level 0 V_{out} vs V_{in} in a calibrated channel, for different clipping values, in photoelectrons	70
3.39 Pulse width measured at different points in the trigger chain	71
3.40 Typical LST layout	74
3.41 Different distances the Cherenkov photons have to go through, depending on the pointing direction	75
3.42 Array trigger scheme [110]	76
4.1 Level 1 working modes [5]	77
4.2 Level 1 general scheme	78
4.3 Schematic of the differential to single-ended stage	79
4.4 Conversion of a Wilkinson splitter made with distributed elements into one made with lumped components	81
4.5 Wilkinson splitters for the L1 Trigger system	81
4.6 Photographs of the Wilkinson splitter prototypes[6]	82
4.7 Measurements of the Wilkinson splitter prototypes[6]	82
4.8 Attenuator schematic	83
4.9 ADG901 block diagram [113]	84
4.10 Adder schematic	85
4.11 Spice simulation of the addition of 3 input pulses (green, yellow and pink). The dark blue line is the result of the addition with ideal electronics, while the red one is the expected output of the real circuit	85
4.12 Measurements of the adder outputs	86
4.13 Measurement of the time over threshold effect [114], considering a 100 mV threshold.	88
4.14 Measured output voltage vs input code for the AD5663R. The output voltages are nearly identical both in the same DAC and in different chips, and linearity is nearly perfect	89
4.15 OR and AND logic gates with diode logic	90
4.16 Generic differential gates using zero-bias Schottky diodes	91
4.17 SPICE simulation of 2, 3 and 6 inputs OR gates	92
4.18 Equivalent circuit of a Schottky diode	92
4.19 SPICE simulation of a 4 input OR gate, with two different Schottky diodes	94
4.20 Spice simulated voltages at the comparator inputs of an OR gate with five inputs, for different values of the resistor in parallel with the diode	94

4.21	Photograph of the manufactured gate test board	95
4.22	Schematic of the gate test board	95
4.23	Measured delay between test board input and output	96
4.24	Measurements of the OR gate differential output pulses, for different resistor values, when there is a 2 ns width pulse at the input	97
4.25	Schematic of the OR gate originally used in the Level 1.	97
4.26	Different front-end boards with similar mezzanines in different positions	99
4.27	Samtec QMSS connectors	99
4.28	Level 1 pin-out	100
4.29	Level 1 PCB stack-up	101
4.30	Level 1 PCB design in Allegro software	102
4.31	Level 1 test board	102
4.32	Level 1 test bench	103
4.33	Photo of the Level 1 test bench	104
4.34	Measurements of the gain for the different channels in mode 4	106
4.35	Measurements of the gain for the different channels in mode 3	107
4.36	Measurements of the gain for the different channels in mode 2	108
4.37	Gain vs pulse width	108
4.38	Latency of the Level 1	109
4.39	Time walk of the Level 1	110
4.40	Jitter of the Level 1	111
5.1	Monte Carlo simulations of duration and time development of showers in the camera.	115
5.2	Sketch of different readout schemes for a slowly developing image	115
5.3	Two threshold timing scheme: Yellow paths represent the additional delay added to the local L triggers to make them fall inside the enabled window initiated by the H trigger (red). By making this delay longer than the propagation latency of the global H trigger it is possible to read also the L triggers which happened just before the H level was exceeded (flashback). Additionally, the enabled window can be extended if the H level is exceeded again inside the first enabled window.	118
5.4	Simulated showers and readout regions for an MST camera	120
5.5	Image and readout region size vs energy	120
5.6	Comparison between different trigger and readout schemes, in terms of the charge fraction read	121
5.7	Simple Hillas reconstruction of a shower image	122
5.8	Ellipse elongation for different readout modes, as function of energy	123

5.9	Level 1 scheme, with the modifications to implement COLIBRI in red	125
5.10	Photos of the Level 1 mezzanine, suitable to implement the COLIBRI scheme. The specific components added for Colibri are inside red circles.	126
6.1	PMT relative transit time for a Hamamatsu R11920 PMT, as a function of the high voltage applied [9]	130
6.2	Ratio of effective area as a function of energy, for different maximum delay dispersion between pixels, with sum and majority trigger strategies[9]. The plots correspond to LST simulations, but for MSTs the effect is also noticeable.	131
6.3	Delay compensation system architecture using a reference signal	132
6.4	Prototype of a delay line with varactors, manufactured and tested at UCM	134
6.5	Output pulses from the prototype delay line with varactors, for different control voltages	135
6.6	Scheme of the delay line based on selectable paths with different lengths	135
6.7	Measured pulses at the output of the delay lines with selectable paths	136
6.8	Characteristics of the output pulses for different delays	137
6.9	Delay meter general scheme [9].	137
6.10	2 inputs LVDS AND gate for the delay meter	138
6.11	Schematic of the width to amplitude converter [9]	138
6.12	Measurements of the width to amplitude converter	139
6.13	Block diagram of the sample, hold and ADC circuit	139
6.14	Waveforms at different points of the sample and hold circuit	140
6.15	ADC measurement for different delays between the leading edges of the reference and the Level 1 output signal	141
6.16	Sketch of the scheme to align pulses and based on rate scans	142
6.17	Possible first 6 iterations to calibrate 1 pixel in every cluster, each one represented as an hexagon in the figure. Orange clusters are under calibration, red clusters are being used as reference, yellow clusters are already calibrated clusters which are disabled to avoid adding more than 2 inputs in the clusters performing rate scans, and blue clusters are the ones not yet calibrated.	143
7.1	Scheme of the interfaces of the TIB with other systems in the camera	146
7.2	Photo of a backplane	147
7.3	Different components of the White Rabbit system [99].	148
7.4	Protocol defined to transmit the trigger type information between the TIB FPGA and the front-end board FPGA	149
7.5	Sketch of the optical fiber from the camera to the basement, with an estimated length of 100 m	153

7.6	Expected LST layout, in a 100 m square rectangular grid	153
7.7	Different distance travelled by the Cherenkov photons depending on the elevation angle θ	154
7.8	Different time of flight depending on the azimuth angle	154
7.9	If the camera trigger signal is synchronized with the trigger condition, the time required to generate the trigger command is variable	156
7.10	If the trigger command is synchronized with the local trigger, the time required to generate the camera trigger signal is fixed	157
7.11	9 LST possible layout	158
7.12	A possible stereo trigger scheme with LSTs and MSTs	159
7.13	Several topologic stereo trigger patterns. 7.13(a), 7.13(b) and 7.13(c) would fire the stereo trigger, but not 7.13(d)	161
7.14	Trigger Interface Board prototype inside the 1U rack box	161
7.15	Internal block diagram of the Trigger Interface Board	162
7.16	Duplex LC connector	163
7.17	Transceiver and housing for 4 SFP transceivers	163
7.18	Schematic of the optical transmitter implemented with a discrete VCSEL	164
7.19	Schematic of optical receiver designed with a discrete photodiode	165
7.20	Xilinx Artix-7 FPGA	167
7.21	TIB firmware architecture	168
7.22	Delay line implemented with a chain of flip-flops	169
7.23	Logarithmic delay line	170
7.24	Diagram of the state machine running in the stretcher modules	170
7.25	Stereo logic block diagram	171
7.26	Stereo trigger delay scheme	172
7.27	State machine which controls the generation of the <i>Armed</i> signal	172
7.28	Trigger output generation in the collector module	173
7.29	State machine which controls the generation and transmission of the trigger type information	173
7.30	Structure of an 8 bit ripple-carry counter	174
7.31	External delay control state machine	176
7.32	Photograph of a Raspberry Pi micro-computer	178
7.33	Slave serial mode FPGA configuration scheme [163]	180
7.34	Block diagram of the TIB power supply system	181
7.35	TIB prototype PCB stack-up	184

7.36 Views of the TIB design and first prototype	185
7.37 Auxiliary boards used for the tests of the Trigger Interface Board	187
7.38 Measurements of the noise in the power supplies and photo of the failing LED	188
7.39 Internal differential clock input buffer and first PLL, in blue	188
7.40 0, 2.5, 12.5, 25 and 30 ns delayed outputs (blue and green) and input (yellow)	189
7.41 4 μ s delayed output (green) and input (yellow)	190
7.42 Several pulse width measurements at the output of the stretchers	190
7.43 Measurements of the signals involved in stereo logic, requiring 3 coincident trigger inputs.	192
7.44 Measurements of the signals involved in stereo logic, showing local trigger requirement and utility of delayed stereo.	193
7.45 Trigger output pulse (blue) and trigger type clock (yellow) and data (green).	194
7.46 Emitter part of an SFP, transceiver, AC coupled [146].	195
7.47 Inverted copy of the input signal (magenta), received analog signal at the input of the comparator (purple) and LVDS output (yellow) of the analog optical link, with a 2 m optical fiber	196
7.48 Inverted copy of the input signal (magenta) and received LVDS output (yellow) of the analog optical link, with a 500 m optical fiber	197
7.49 Input signal (yellow) and delayed 0 (green), 50, 100, 150 and 200 steps of 2 ns (blue) with DS1123LE-200.	198
7.50 Delay measurement with 3D3428 delay line	199
 8.1 Simulation results of the topologic scheme for the MAGIC telescopes	204
8.2 Sectorization scheme	205
8.3 Triangulation scheme	207
 A.1 L1: Schematic Index	210
A.2 L1: General Schematic	211
A.3 L1: Differential to Single-Ended (channels 0,1, and 2)	212
A.4 L1: 3 branches splitter	213
A.5 L1: 4 inputs adders	214
A.6 L1: Differential to Single-Ended (channels 3, 4 and 5)	215
A.7 L1: 2 branches splitter	216
A.8 L1: Attenuator	217
A.9 L1: LVDS OR gate	218
A.10 L1: comparators	219

A.11 L1: LVDS AND gate	220
A.12 L1: Width to Amplitude converter	221
A.13 L1: Read Pulse Amplitude circuit	222
A.14 TIB: FPGA pins	224
A.15 TIB: FPGA power filtering	225
A.16 TIB: JTAG connector	226
A.17 TIB: Raspberry Pi pins	227
A.18 TIB: LVDS to LVPECL translators	228
A.19 TIB: LVPECL to LVDS translators	229
A.20 TIB: Optical transceivers to/from neighbours	230
A.21 TIB: Optical transceivers to/from calibration box	231
A.22 TIB: RJ45 connectors	232
A.23 TIB: External delays	233
A.24 TIB: Thermometer	234
A.25 TIB: Power supplies	235
A.26 TIB: Power monitor LEDs, mechanical holes and grounding	236
C.1 Free MTBF calculator, from ALD [173]	243

List of Tables

2.1	Comparison chart of the main kinds of photodetectors suitable for IACTs	25
2.2	Characteristics of several readout schemes based on analog memories	27
3.1	Delays of the trigger system	66
3.2	Power consumption for one cluster	72
3.3	Summary of camera analog trigger parameters	73
4.1	Contributions to the sums for the different channels and modes, and gains in the differential to single-ended stage	80
4.2	Distribution of the input channels among the adders and control logic for working-mode switching	83
4.3	Mode codification	84
4.4	Noise measurements of the Level 1 prototype, for two similar manufactured boards..	105
7.1	Pinout definition of the RJ45 connectors between the TIB and the clock board and the central backplane	151
7.2	Slow control registers	177
7.3	Raspberry Pi GPIO pinout	179
7.4	Expected power consumption according to datasheets and FPGA simulations	182
7.5	Characteristics of the power supplies modules	183
7.6	Operating temperature range of the electronic components in the TIB	184
7.7	Measured DC voltage and AC coupled RMS voltage for the different voltage rails present in the TIB	186
7.8	Measured rates using the ITR counters	195
B.1	Level 1 bill of materials per cluster: Component costs in €	238
B.2	Level 1 bill of materials per cluster: Mezzanine manufacturing costs in €	239
B.3	Level 1 mezzanine production fixed costs in €	239

B.4 Bill of materials of 1 Trigger Interface Board	242
B.5 Fixed costs of the Trigger Interface Board	242
C.1 Reliability estimation for the Level 1, only components	245
C.2 Reliability estimation for the Trigger Interface Board	247

List of Acronyms

- **4PST**: 4 Pole, Single Throw.
- **AGN**: Active Galactic Nucleus.
- **APC**: AstroParticule et Cosmologie.
- **APD**: Avalanche PhotoDiode.
- **API**: Application Programming Interface.
- **ASIC**: Application Specific Integrated Circuit.
- **CANGAROO**: Collaboration of Australia and Nippon for a GAMMA-Ray Observatory in the Outback.
- **CCD**: Charge-Coupled Device.
- **CCM**: Concordance Cosmological Model.
- **Ciemat**: Centro de Investigaciones Energéticas, Medioambientales y Tecnológicas.
- **COLIBRI**: Concept for an Optimized Local Image Building and Readout Infrastructure.
- **CTA**: Cherenkov Telescope Array.
- **DESY**: Deutsches Elektronen Synchrotron
- **DRS**: Domino Ring Sampler.
- **EAS**: Extended Air Shower.
- **ECL**: Emitter-Coupled Logic. A high-speed integrated circuit bipolar transistor logic family.
- **EGRET**: Energetic Gamma-Ray Experiment Telescope.
- **ESFRI**: European Strategy Forum for Research Infrastructures.
- **ESO**: European Southern Observatory.
- **ETSIT**: Escuela Técnica Superior de Ingenieros de Telecomunicación
- **eV**: Electronvolt, $\approx 1.6 \times 10^{-19}$ J.
- **FACT**: First GAPD Cherenkov Telescope.
- **FIT**: Failure In Time.
- **FPGA**: Field Programmable Gate Array.
- **FR4**: A composite material composed of fiberglass cloth and an epoxy resin binder that is Flame Resistant. Commonly used for PCB manufacturing.
- **GAE-UCM**: Grupo de Altas Energías - Universidad Complutense de Madrid

- **GAPD:** Geiger-mode Avalanche PhotoDiode. Another name for SiPM.
- **GeV:** Gigaelectronvolt, $\approx 1.6 \times 10^{-10}$ J.
- **GLAST:** Gamma-ray Large Area Space Telescope. Also known as Fermi satellite.
- **GMR-UPM:** Grupo de Microondas y Radar - Universidad Politécnica de Madrid.
- **GPIO:** General Purpose Input/Output.
- **GRANAT:** International Astrophysical Observatory, in Russian.
- **GRB:** Gamma-Ray Burst.
- **HDMI:** High-Definition Multimedia Interface.
- **HEGRA:** High Energy Gamma-Ray Astronomy.
- **HESS:** High Energy Stereoscopic System.
- **HPD:** Hybrid PhotoDetectors.
- **I2C:** Inter-Integrated Circuit. A serial bus used for low-speed electronic devices.
- **IACT:** Imaging Atmospheric Cherenkov Telescope.
- **ICC-UB:** Institute of Sciences of the Cosmos, Universidad de Barcelona.
- **IFAE:** Instituto de Física de Altas Energías.
- **ITR:** Individual Telescope Rate.
- **LAN:** Local Area Network.
- **LHC:** Large Hadron Collider.
- **LPNHE:** Laboratoire de Physique Nucléaire et des Hautes Énergies.
- **LST:** Large Sized Telescope.
- **LUPM:** Laboratoire Univers et Particules de Montpellier.
- **LUT:** Look Up Table.
- **LVDS:** Low Voltage Differential Signaling. An electrical digital signaling standard that can run at very high speeds over differential pairs.
- **LVPECL:** Low Voltage Positive Emitted-Coupled Logic. A variant of PECL using a positive +3.3V instead of +5V supply.
- **MAGIC:** Major Atmospheric Gamma-ray Imaging Cherenkov telescopes.
- **MISO:** Master In Slave Out. One of the typical lines in an SPI interface.
- **MOSI:** Master Out Slave In. One of the typical lines in an SPI interface.

- **MPI**: Max Planck Institute.
- **MPPC**: Multi-Pixel Photon Counter. Another name for SiPM.
- **MST**: Medium Sized Telescope.
- **MTBF**: Middle Time Between Failures.
- **NECTAr**: New Electronics for the Cherenkov Telescope Array.
- **NSB**: Night Sky Background.
- **OPC-UA**: Open Connectivity - Unified Architecture
- **OSO**: Orbital Solar Observatory.
- **PDE**: Photon Detection Efficiency.
- **PECL**: Positive Emitter-Coupled Logic. A variant of ECL using a positive 5 V power supply instead of a negative 5.2 supply.
- **PET**: Positron Emission Tomography.
- **PLL**: Phase Locked Loop.
- **PMT**: Photomultiplier Tube.
- **PPS**: Pulse Per Second.
- **QE**: Quantum Efficiency.
- **ROI**: Region Of Interest.
- **SAM**: Swift Analog Memory.
- **SD**: Secure Digital.
- **SFP**: Small Form Factor Pluggable.
- **SIGMA**: Système d'Imagerie Gamma à Masque Aléatoire.
- **SiPM**: Silicon Photomultiplier.
- **SP4T**: Single Pole 4 Throw.
- **SPI**: Serial Peripheral Interface bus.
- **SPST**: Single Pole Single Through.
- **SSH**: Secure SHell.
- **SST**: Small Sized Telescope.
- **TDC**: Time to Digital Converter.
- **TeV**: Teraelectronvolt, $\approx 1.6 \times 10^{-7}$ J.

- **TIB:** Trigger Interface Board.
- **UAB:** Universidad Autónoma de Barcelona.
- **UART:** Universal Asynchronous Receiver/Transmitter.
- **UB:** Universidad de Barcelona.
- **UCM:** Universidad Complutense de Madrid.
- **UPM:** Universidad Politécnica de Madrid.
- **UTC:** Universal Time Coordinated.
- **VCSEL:** Vertical-Cavity Surface-Emitting Laser.
- **VERITAS:** Very Energetic Radiation Imaging Telescope Array System.
- **VHDL:** VHSIC (Very High Speed Integrated Circuit) Hardware Description Language.

Chapter 1

Introduction.

This thesis presents the author's contribution to the trigger systems used in Imaging Atmospheric Cherenkov Telescopes (IACTs). These kind of telescopes are essential for the study of the γ -rays sources in the universe. During the last decades, several experiments and projects have developed IACTs which have resulted in important scientific discoveries. As the basic technologies were being improved, the new IACTs have been increasingly powerful and sensitive. The next step of the international γ -ray astronomy community consists of building a large array with many IACTs, using the latest high technology to build the best telescopes ever, and thus covering all the γ -ray spectrum from all the sources in all the sky. This is the target of the Cherenkov Telescope Array (CTA) consortium. In order to reach this goal, new trigger systems are required for the new telescopes. In this framework, the main objective of this thesis is to develop some contributions to the trigger systems for some CTA IACTs, which will help to optimize their sensitivity and performance.

To reach this aim, a top-down methodology has been followed. First, the place of the trigger systems in the IACTs architecture and its relation with the other main systems was defined. Then the different subsystems composing the trigger system were defined, and finally, the circuits, PCBs, firmware, etc. were designed, manufactured and tested. The tests follow the inverse path, first the different subsystems are tested individually, then the whole trigger system is tested, later a whole camera must be integrated and tested, and finally the complete telescope must be tested too.

This thesis follows a quite similar structure: first an extensive introduction presents the γ -ray astronomy, the IACTs and their main technological issues, then the whole trigger system is described, and later the specific subsystems and technical developments done by the author of this thesis and his collaborators are explained. In this way, the thesis has been organized as follows.

- Chapter 2 is an introduction to the Cherenkov telescopes field. In first place it explains the ultimate purpose of the Cherenkov telescopes: to observe γ -ray emissions coming from certain astronomical objects with the aim of obtaining scientific data about them. In order to do so, the γ -rays can be detected directly, or by means of the Cherenkov light showers which they produce in the atmosphere. In the last case, IACTs are required to detect such light [1]. These kind of telescopes are complex devices composed of many subsystems which are briefly described in this chapter. Finally, the Cherenkov Telescope Array (CTA) project is presented, being the framework for the devices developed in this thesis. An introduction to the CTA concept was published in [2] by all the CTA consortium members, including myself.

- Chapter 3 is focused in the trigger system. First, the generic components of an IACT trigger system are explained, as well as the most common trigger strategies used in currently active IACTs. Then, the specific trigger system developed for CTA by the author at UCM and other partner institutions is described, including all the different hardware modules developed and measurements of the complete system. This description of the developed trigger system was published in [3], and presented in international congress like in [4].
- Chapter 4 is even more specific, being focused in the Level 1 trigger subsystem. This subsystem is one of the main contributions of the author, and as such it is described in depth. The Level 1 trigger system alone was important enough to deserve a dedicated publication in [5]. Moreover, some subsystems like the splitters were presented at a congress [6], and the LVDS OR gate resulted in the patent [7].
- Chapter 5 presents an original trigger and readout scheme based on partial readings of the camera. It can potentially reduce the amount of data taken while improving the quality of the images and incrementing the telescope performance, and it can be implemented with the presented trigger system. The concept was proposed by C. Lindsay Naumann from the Laboratoire de Physique Nucléaire et des Hautes Énergies (LPNHE), while the technical implementation was developed by myself and by G. Martínez from the Centro de Investigaciones Energéticas, Medioambientales y Tecnológicas (CIEMAT), as it is described in [8].
- Chapter 6 analyzes the problems caused by the different delays introduced by the photodetectors over the trigger systems like the one presented in this thesis. Then a technical solution feasible to implement with the existing hardware is described. Both the analysis and the proposed solution were published in [9].
- Chapter 7 presents another module of the trigger system: the Trigger Interface Board. This subsystem is in charge of triggering the camera when there is a local trigger, but also when a trigger is required for calibration or other reasons. Additionally, it implements a multi-telescope trigger scheme for the largest telescopes of CTA.
- Chapter 8 summarizes the conclusions of the thesis and presents the future working lines regarding the trigger systems of CTA.

Finally, several appendix are placed at the end of this thesis, gathering specific information about electrical schematics, costs, and reliability of the different systems presented.

Chapter 2

Ground based γ -ray astronomy and Cherenkov telescopes

This chapter intends to introduce the reader to the γ -ray astronomy and to the different techniques used to detect γ radiation from outer space. One of this techniques, known as Cherenkov technique, requires complex telescopes to be developed. These telescopes are composed of many different subsystems with strict requirements, involving important technological challenges. This chapter presents the most noticeable issues, with the aim to prepare the reader for the next chapters, which are focussed in the trigger subsystems and constitute the core of this thesis.

2.1 γ -ray astronomy

Gamma-ray astronomy intends to observe cosmic objects emitting photons with an energy higher than 1 MeV¹ and up to 1 PeV² or even larger which come from certain astronomical objects. These very high energetic photons are not generated by conventional thermal phenomena (it does not exist anything hot enough), but by other astronomical accelerating mechanisms much more violent or exotic [10], which are typically related with massive compact objects such as neutron stars or black holes. These objects typically act as giant particle accelerators, speeding up charged particles (protons, electronos, etc.) up to relativistic speeds. Then, these accelerated charged particles, known as cosmic rays, can cause γ -ray emissions by bremsstrahlung, synchrotron, curvature radiation, inverse Compton effect or neutral pion decay[11]. Some of the objects able to unchain these processes are presented below:

Supernova remnants

When a star explodes producing a supernova, it expels much of its material at speeds as high as 10% of the speed of light. This ejected material moves much faster than the sound speed in the gases of the interstellar medium, forming a strong shock wave which heats the upstream plasma up to millions of K. These shock waves can also accelerate particles by first

¹1MeV = $1 \cdot 10^6$ eV $\cdot 1.6 \cdot 10^{-19} \frac{J}{eV}$ = $1.6 \cdot 10^{-13}$ J
² $1.6 \cdot 10^{-4}$ J

and second order Fermi mechanisms [12]. The magnetic field irregularities in the shock front keep scattering the charged particles back and forth, crossing the same shock many times and thus getting very much accelerated. Due to this process, supernova remnants can originate very high energy cosmic rays up to 10^{15} eV, being considered the major source of galactic³ cosmic rays. These cosmic rays, being composed of accelerated charged particles, can interact with surrounding photons by inverse Compton effect, transferring the energy to the photons and thus generating γ -ray emission.

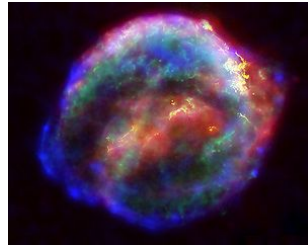


Figure 2.1: X-ray, optical and infrared composite of Kepler's supernova remnant

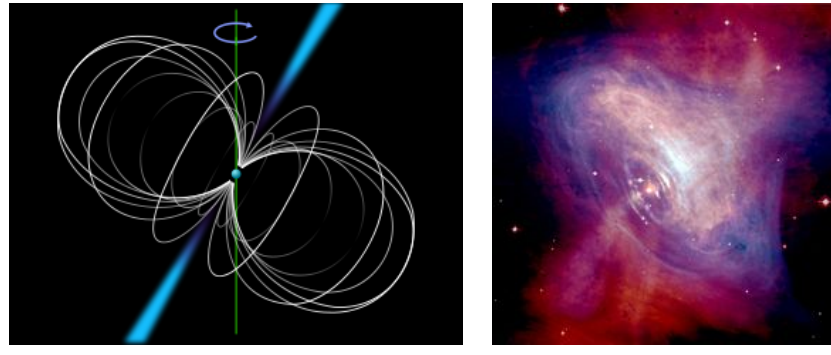
Pulsars

Pulsars are formed when the core of a massive star is compressed during a supernova and collapses into a neutron star. The neutron star retains most of the angular momentum of the original star but with only a small fraction of its radius, so the new object has to rotate very fast. The rotation of the protons and electrons on the star surface originates a very strong magnetic field, which accelerates the charged particles emitting a beam of radiation along the magnetic axis of the pulsar. Additionally, as it is shown in figure 2.2(a), the pulsar spins around an axis not necessarily being aligned with the magnetic axis, which produce the periodical change in the beam direction and thus the periodical variation of the radiation intensity measured from the Earth. The very highly accelerated particles moving along curve trajectories affected by the strong electromagnetic field produce γ -rays in a natural way by bremsstrahlung and synchrotron effects.

Active Galactic Nucleus

Active galactic nucleus (AGN) are compact extragalactic objects that emit very luminous electromagnetic radiation[13]. They consist of a central supermassive black hole (10^6 to 10^9 solar masses) which attracts the gas and the stars that are too close. Before being completely absorbed by the black hole, the attracted matter spins around it, forming an accretion disc. The matter in the accretion disc is heated because of the friction becoming plasma, emitting light and generating a magnetic field. Sometimes, this magnetic field collimates two extremely powerful jets of plasma emerging from the center of the AGN and perpendicular to the accretion disc. The mechanics behind the creation of the jets is still not clear for the scientific community, but the most extended hypothesis is that the jets are composed of an electrically neutral mixture of electrons, positrons and protons moving at relativistic speeds over thousands of

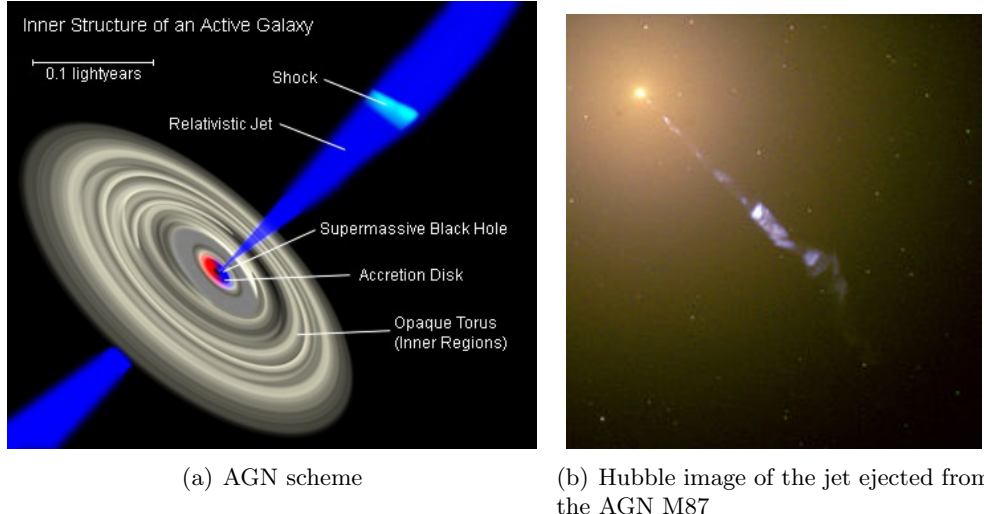
³In γ -ray astronomy is common to distinguish between emissions from the Milky Way (galactic) or from whatever other place in the universe (extragalactic)



(a) Pulsar scheme with the magnetic field lines, the beams and the rotation axis
 (b) X-ray and optical composite of Crab Pulsar Nebula

Figure 2.2: Schematic and observation of a pulsar

light years. These particles, in turn produce γ -ray emission by inverse Compton effect and synchrotron emission. Quasars and Blazars are different kinds of AGNs.



(a) AGN scheme

(b) Hubble image of the jet ejected from the AGN M87

Figure 2.3: Scheme and observation of an AGN

X-ray binaries and microquasars

A microquasar is a galactic object with similar characteristics than the ones observed in the quasars but in a reduced scale. In this way, while in the case of AGNs the compact object is a supermassive black hole, in the case of microquasars it is just a neutron star or a small black hole with only several solar masses. In fact, microquasars are binary systems composed of a compact object and a massive star. When the star and the compact object are close enough, the last accretes matter from the second forming an accretion disc which emits light and generates a magnetic field as in the case of AGNs. In the same way, microquasars also have jets and emit γ -rays. The main difference is that, as the scale is much reduced, phenomena that last centuries in the AGNs last days in the case of microquasars.

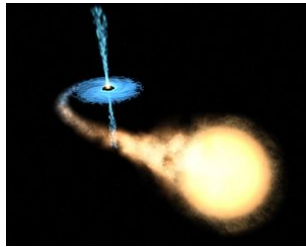


Figure 2.4: X-ray binary, artist impression

Gamma Ray Bursts

Gamma Ray Bursts (GRBs) are very bright flashes of radiation with spectral energy distributions peaking in the γ -ray band [10]. The emission lasts from ten milliseconds to several minutes and is usually followed by a longer-lived “afterglow” emitted at longer wavelengths (X-ray, ultraviolet, etc.). GRBs are believed to be associated to supernova or hypernova explosions and they are considered as the brightest electromagnetic events in the universe. The sources of most GRBs are thousands of millions of light years from the Earth, so from the received energy it can be deduced that a typical burst releases as much energy in a few seconds as the sun in its entire lifetime. Due to the short duration and the huge distances of γ -ray bursts from Earth, this phenomenon is really difficult to study, and not much is known about the specific physical mechanisms involved.

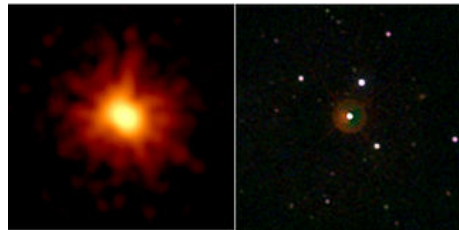


Figure 2.5: Image of GRB 080319B in X-ray (left) and optical (right)

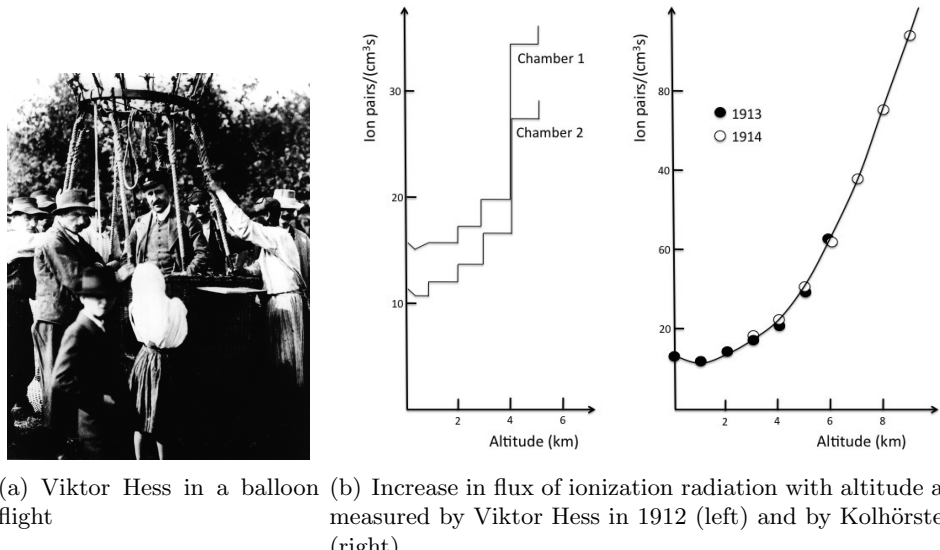
Dark matter annihilation, according to the most accepted models

From the study of the dynamics of galaxies and galaxy clusters, and the gravitational lensing effects, it can be deduced that in the universe there is much more mass than we can see. The existence of dark matter which neither emits light nor interacts with the light emitted by other objects is a widely accepted fact. However, the dark matter composition is still a mystery. There are several hypothesis about the nature of the dark matter, complying with the Concordance Cosmological Model (CCM), currently accepted by most of the scientific community. In order to verify these hypothesis there are several researches currently taking place. Some of them try to directly produce dark matter particles in accelerators like LHC. Others try to find evidences of dark matter among the usual matter in the Solar System. And finally, others do not try to detect directly the dark matter, but the Standard Model particles generated from dark matter particles annihilation or decay. Annihilation of dark matter can not happen fast (otherwise all dark matter would have already disappeared), but

it could happen in certain conditions. The products which should be obtained from dark matter annihilation depend strongly on the precise dark matter model, and they can range among protons, electrons, neutrinos, photons of different energies including γ -rays and their corresponding antiparticles. Observing the places in the universe where the gravitational effects of dark matter are more evident (the galactic center, galaxy clusters, etc.) and looking for the annihilation products of this dark matter, it should be possible to confirm or reject different models. As several of the most accepted dark matter models postulate the emission of high energy γ -rays, the observations in this range become a crucial tool to find out the nature of more than a half of all the matter in the universe [14], [15].

2.2 Gamma-ray detection techniques

Unlike astronomical observations at other frequencies like the optical, infrared, or radio ones, observing γ -rays has an additional difficulty. Fortunately for the life in the Earth, the atmosphere absorbs most of the gamma radiation, making direct observation at ground level impossible or, at least very challenging. First experiments done by Viktor Hess in 1911, 1912 and 1913 in balloon flights showed that the flux of ionizing radiation (cosmic rays, γ -rays, X-rays, etc.) increases with height as it is shown in figure 2.6(b).



(a) Viktor Hess in a balloon flight (b) Increase in flux of ionization radiation with altitude as measured by Viktor Hess in 1912 (left) and by Kolhörster (right)

Figure 2.6: First detections of ionization radiation in the atmosphere

In spite of this important difficulty, two techniques are currently available to observe the γ -rays coming from outer space: the **direct observation** by particle detectors on board of satellites, and the **indirect detection** by ground-based detectors using the **Cherenkov technique**. Both are explained in the following subsections.

2.2.1 Direct detection by on-board satellite detectors

Of course, the most direct solution to detect cosmic γ -rays is to measure them where they have not been absorbed yet, that is, out of the atmosphere. In the 1960s the first satellites with calorimeters able to detect gamma rays were launched. Oddly enough, these first satellites were not aimed to study any astrophysical object but to detect nuclear weapon tests during the Cold War years. Thus, in 1961 the Explorer XI discovered the first γ -rays outside the atmosphere. In 1967 the satellites of Vela Network detected the first Gamma Ray Burst in history. In 1968, the OSO-III (Orbital Solar Observatory) obtained the first map of the γ -ray emission coming from Milky Way at energies above 30 MeV, and in 1972 OSO-VII discovered the spectral lines of nuclear interaction in solar flares.

These first detectors had very limited angular resolution, but this characteristic was improved in the following experiments. In this way, in the 90's the experiment SIGMA (Système d'Imagerie Gamma à Masque Aléatoire), on board of the GRANAT satellite, identified around 30 sources in the center of the Milky Way and the EGRET instrument (Energetic Gamma Ray Experiment Telescope [16]), on board of the American satellite Compton Gamma Ray Observatory discovered more than 270 sources of γ -ray emission between 30 MeV and 30 GeV.

Nowadays, the Fermi Gamma-ray Space Telescope (formerly named the Gamma-ray Large Area Space Telescope, GLAST [17]), launched in 2008, has discovered and characterized 1873 sources in the 100 MeV to 100 GeV range [18] and it is still operating, discovering new sources and improving the knowledge of the already known ones every day.

2.2.2 Ground-based detectors: the Cherenkov technique

As most of the gamma radiation is absorbed by the atmosphere, direct detection at ground level is impossible. However, it is possible to detect the effect of γ -rays in the atmosphere. When a primary γ -ray first interacts with a molecule of the atmosphere it generates an electron-positron pair. These two particles will further interact with other atmosphere molecules, loosing a fraction of their energy by the bremsstrahlung effect, and thus emitting a lower energy γ -ray. The new γ -rays create more electron-positron pairs and generate even lower energy γ -rays and the process repeats until the produced γ -rays have so low energy that they cannot produce new electron-positron pairs. In this way an Extended Air Shower (EAS) is created, as it is represented in an schematic way in figure 2.8(a).

The secondary particles generated in this process are very highly energetic, so they move very fast. When the speed of this charged particles is higher than the speed of light in the atmosphere, Cherenkov light is produced. This condition is met if the medium presents a refractive index $n > 1$ and the particle velocity is $v > c/n$. A charged particle moving through a transparent medium polarizes it instantaneously. If the particle moves more slowly than light in the medium, the net polarization field is null due to the symmetric arrangement of the dipoles. However, if the particle speed is higher than the light speed in the medium, then the polarization gets asymmetric and a net field is created (see figure 2.9(a)). Since the field inductor (the charged particle) is faster than the field propagation itself, then a shock wave of in-phase reorientation of dipoles is generated, which originates the Cherenkov photon emission (figure 2.9(b)) [15].

The spectrum of the Cherenkov light approximately depends on the wavelength as $1/\lambda^2$, but once the atmospheric attenuation is taken into account, the resulting spectrum peaks around the

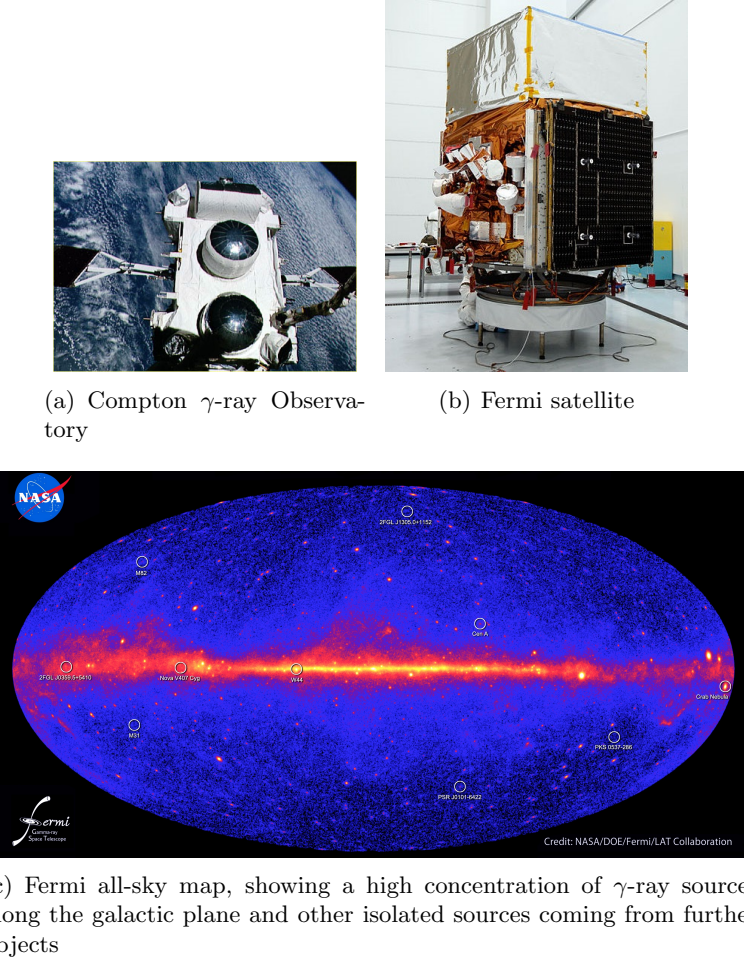


Figure 2.7: History of gamma-ray astronomy by direct detection.

near UV and blue range of the visible spectrum. Attending to the geometrical argument shown in figure 2.9(b), the Cherenkov photons are emitted in a cone characterized by a certain angle θ , known as Cherenkov angle. θ depends on the refractive index which, in turn depends on the height. Thus, θ is less than 1° above 8 Km height, 1° at 8 Km height and 1.4° at sea level. Nevertheless, the higher the shower occurs, the more space the cone has to spread and, at the end, the Cherenkov photons cast on a circle of roughly 120 m radius, whatever the height at which the EAS happened (typically at 10 Km high).

A typical shower initiated by a 100 GeV γ -ray generates several hundreds of thousands of Cherenkov photons. Imaging Atmospheric Cherenkov Telescopes (IACTs) have the global shape of an optical telescope, with a primary reflector of an overall parabolic shape, and a camera in the focus of the paraboloid. When such a telescope is placed in the light pool the reflector will collect part of the Cherenkov photons and will reflect them in the pixelized camera (with typical pixel size of 0.1° , corresponding to 2-3 cm diameter), where an image of the shower is formed, showing an approximate elliptical shape, as sketched in figure 2.10. Analysing these images it is possible to obtain the so-called Hillas parameters [19], which are directly related with the meaningful physical parameters of the original γ -rays which generated the showers, such as their energies and directions.

2. Ground based gamma-ray astronomy and Cherenkov telescopes

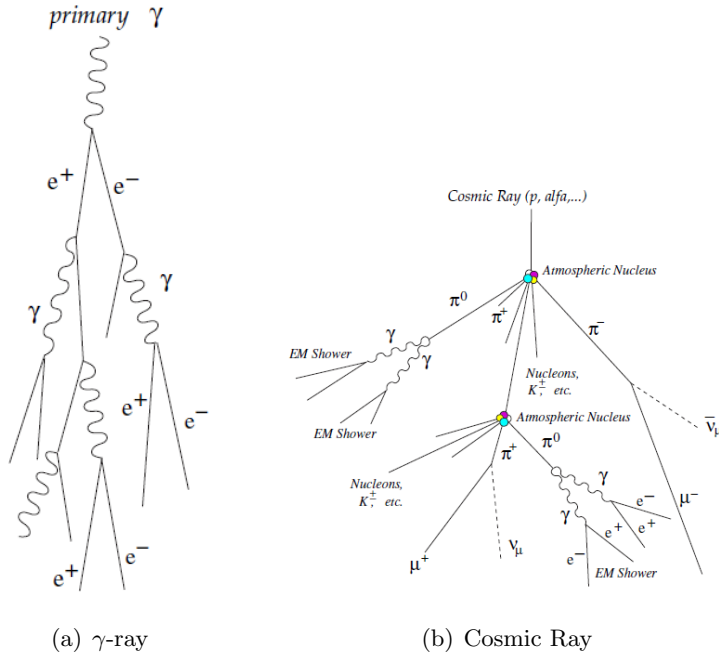


Figure 2.8: Extended Air Showers generated by γ -rays and cosmic-rays

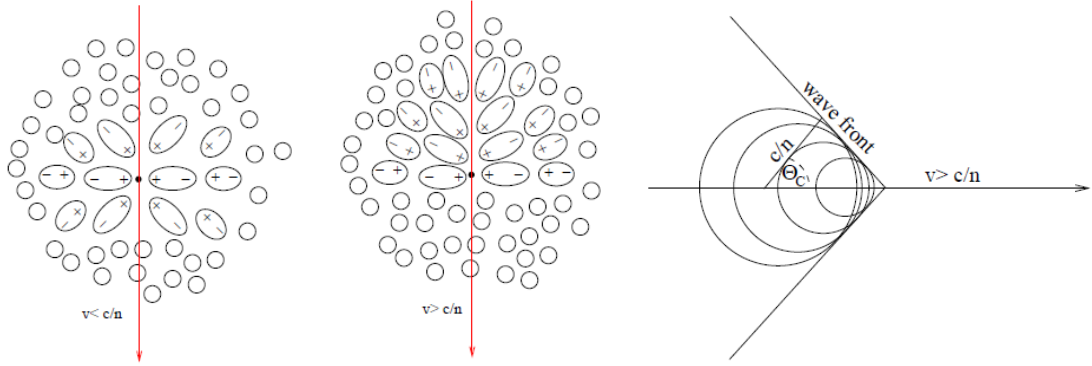


Figure 2.9: Schematic simplification of the Cherenkov effect

In spite of the underlying idea is not very difficult, detecting the Cherenkov light corresponding to an air shower generated by a γ -ray is not an easy task. Cherenkov light pool is very faint, having Cherenkov images at the camera with no more than a few thousand photons, and the duration is very short, between 2.5 and several tens of nanoseconds. This makes necessary the use of very sensitive and fast photodetectors like the ones described in section 2.3.3, as well as fast and low noise electronics, capable to detect and save the interesting images. There is a special background component that an IACT has to face with when detecting low energy γ -rays, which yield a small number of Cherenkov photons (typically below 500). This background comes from the fact that the environment is not totally dark (there is always a certain amount of light coming from stars,

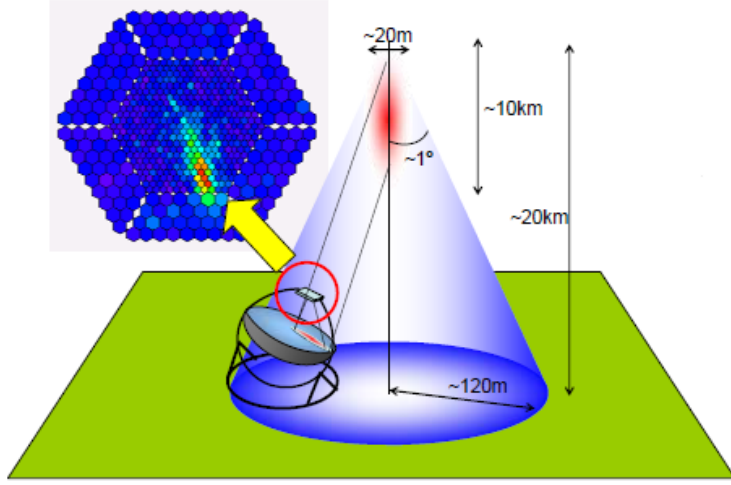


Figure 2.10: Basic scheme of Cherenkov technique [20].

the moon, human activities, etc..., which form the so-called Night Sky Background (NSB)), and this background light can mimic γ -ray induced showers of small energy.

Besides this difficulty, γ -rays are not the only ones which generate extended air showers. Cosmic rays, mainly composed of protons and alpha particles also generate showers (so-called hadronic showers) with their associated Cherenkov light pools (see figure 2.8(b)) and they are much more common than γ -rays in a typical relation 10000:1. The Cherenkov light pool generated by the cosmic rays is originated in the electromagnetic (EM) sub-showers of the hadronic showers (see fig. 2.8(b)), so that the Cherenkov images formed at the telescope camera are not so uniform and elliptic-like as the γ -ray showers, as shown in fig. 2.11. Additionally, the cosmic rays, in contrast to the γ -rays, are charged particles, so that they are deflected by interstellar magnetic fields, thus when they arrive to the Earth, they do not point anymore to their source. Therefore, when a telescope is pointing at a given object, the ellipse-like image from a γ -ray shower has its major axis pointing to the camera center, while this is not the case for the cosmic-ray images. This two special features of the Imaging Cherenkov technique allows to strongly suppress the cosmic-ray background and has permitted the advent of the γ -ray ground-based astronomy as a new branch of astronomy.

2.2.3 Sensitivity of an IACT

The main purpose of an IACT is to collect Cherenkov shower images caused by γ -rays coming from astronomical objects such as the ones mentioned in section 2.1. The number of γ -ray induced showers caused by a source depends on the flux of γ photons from that source which reach the Earth atmosphere. The more γ photons, the more Cherenkov showers detected by the IACT and the simpler to detect the source. In this way, the sensitivity of an IACT is defined as the minimum detectable flux of γ -rays which can be detectable in 50 hours of observation, with a statistic significance of 5 standard deviations. The statistic significance of an observation is used to decide if an excess of Cherenkov events coming from a certain direction in the space corresponds to a γ -ray source or, on the contrary, it can be caused just by a statistical fluctuation. In fact, an statistic significance

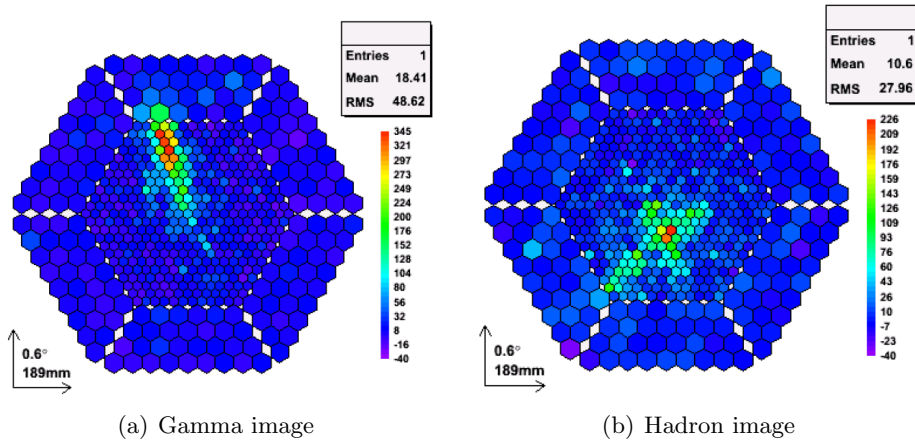


Figure 2.11: Images recorded by the camera of MAGIC-I telescope, corresponding to a γ -ray and a shower originated by an hadron

higher or equal to 5 standard deviation is widely accepted as an evidence of the existence of a γ -ray source.

The calculation of the statistic significance of an IACT observation begins with two observations: one of them pointing to the source under study and other pointing to a dark area of the sky to estimate the background. Naming N_{on} to the number of events captured when pointing to the source and N_{bkg} to the number of events captured when pointing to the dark area, N_{on} will be slightly higher than N_{bkg} if the source emits γ -rays. Then, an excess of γ -like events is defined as the difference between N_{on} and N_{bkg} (equation 2.1).

$$N_{ex} = N_{on} - N_{bkg} \quad (2.1)$$

The significance S of N_{ex} is defined as shown in equation 2.2, being $\sigma(N_{ex})$ the standard deviation of N_{ex} .

$$S = \frac{N_{ex}}{\sigma(N_{ex})} \quad (2.2)$$

$\sigma(N_{ex})$ can be expressed in terms of $\sigma(N_{on})$ and $\sigma(N_{bkg})$ as shown in equation 2.3:

$$\sigma(N_{ex}) = \sqrt{\sigma^2(N_{on}) + \sigma^2(N_{bkg})} \quad (2.3)$$

As the γ ray detections follow a Poisson distribution, equation 2.3 can be simplified as equation 2.4:

$$\sigma(N_{ex}) = \sqrt{N_{on} + N_{bkq}} \quad (2.4)$$

As the number of background events is much higher than the excess events, it is possible to approximate N_{on} by N_{bkg} in equation 2.4.

$$\sigma(N_{ex}) = \sqrt{2 \cdot N_{bkg}} \quad (2.5)$$

Introducing equation 2.4 in 2.2, equation 2.6 shows an expression for the significance in terms of N_{on} and N_{bkg} :

$$S = \frac{N_{ext}}{\sqrt{2 \cdot N_{bkg}}} = \frac{N_{on} - N_{bkg}}{\sqrt{2N_{bkg}}} \quad (2.6)$$

Finally, with the aim to compare the significance of different sources, it is common to ignore the factor 2 and use equation 2.7 instead of 2.6 [21]:

$$S = \frac{N_{on} - N_{bkg}}{\sqrt{N_{bkg}}} > 5 \quad (2.7)$$

Equation 2.7 is simple and very convenient, but it includes several approximations. In order to be mathematically rigorous, equation 17 of Li&Ma paper [22] is preferred. It is also worth to notice that the sensitivity is defined for 50 hours of observation, but a source can be observed during more time in order to increase the significance and thus detect the source or analyze it more in detail.

2.2.3.1 Integral sensitivity

The definition of sensitivity presented does not take into consideration the energy of the γ -rays, but all the events are taken into account. However, the sensitivity of the IACTs depends on the energy range, being optimized for a certain range and being reduced for weaker energies (because the showers are smaller and more difficult to detect). Therefore, it is interesting to represent the sensitivity as a function of the energy range. In this way, the integral sensitivity is defined as the minimum detectable flux of γ -rays from a source above a given energy, which can be detectable in 50 hours of observation, with an statistic significance of 5 standard deviations. For instance, figure 2.12 shows the integral sensitivities of the MAGIC 1 telescope and the MAGIC stereo system [21].

2.2.3.2 Differential sensitivity

To evaluate the performance of an IACT along a large energy range, the sensitivity can be calculated in narrow bins of energy. To compute this sensitivity the events are classified in several bins of energy and, for each of them, the N_{ex} counts the number of events in the energy range, considering all the others as background. In this way, the differential sensitivity is defined as the flux of the source in a given energy range for which an statistic significance of 5 standard deviations is obtained after 50 hours of observation. Figure 2.13 shows the differential sensitivity of the MAGIC telescopes.

Both in the case of differential and integral sensitivity, it is also very common to normalize the flux to the one of the Crab Nebula, which is very well characterized in the different energy ranges and used as standard candle.

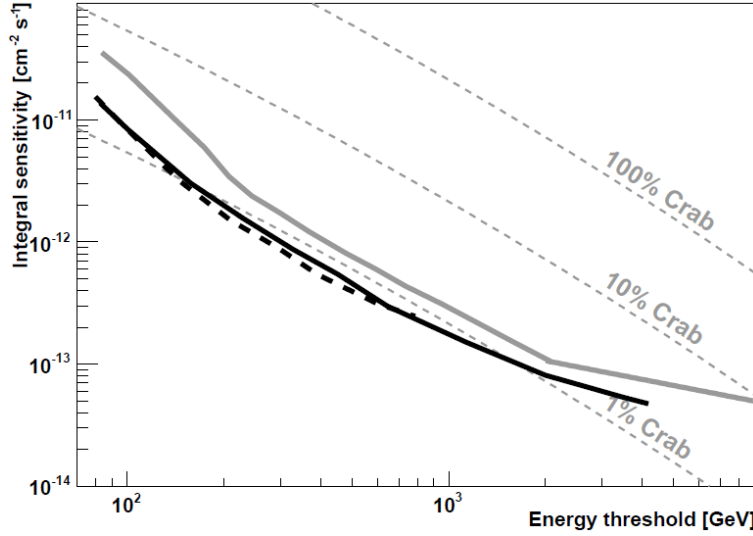


Figure 2.12: Integral sensitivity of the MAGIC stereo system. Black solid line represents the measured sensitivity, black dashed line the expected sensitivity from the MonteCarlo simulations, and grey line represents MAGIC-I integral sensitivity when working alone [21]. The flux is expressed in photons $\cdot cm^{-2} \cdot s^{-1}$.

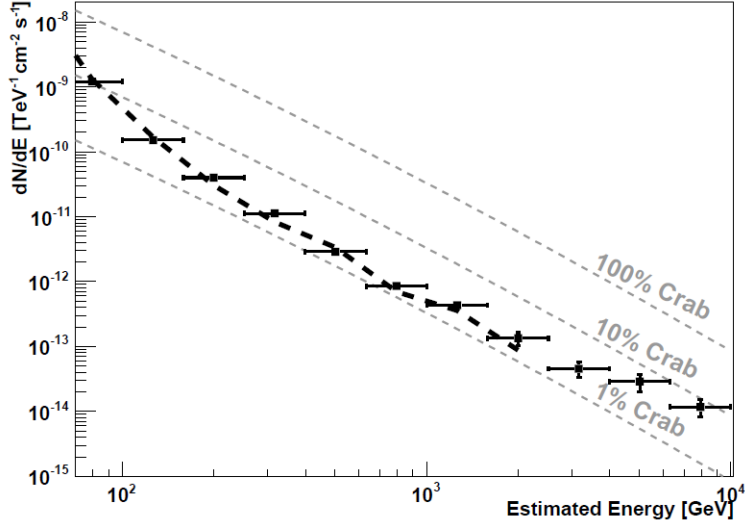


Figure 2.13: Differential sensitivity of the MAGIC stereo system , expressed in $TeV \cdot cm^{-2} \cdot s^{-1}$. Black points represent the differential sensitivity, black dashed line represents the differential sensitivity expected from the simulations, and the horizontal error bars represent the size of the bins in estimated energy [21]

2.2.3.3 Effective collection area

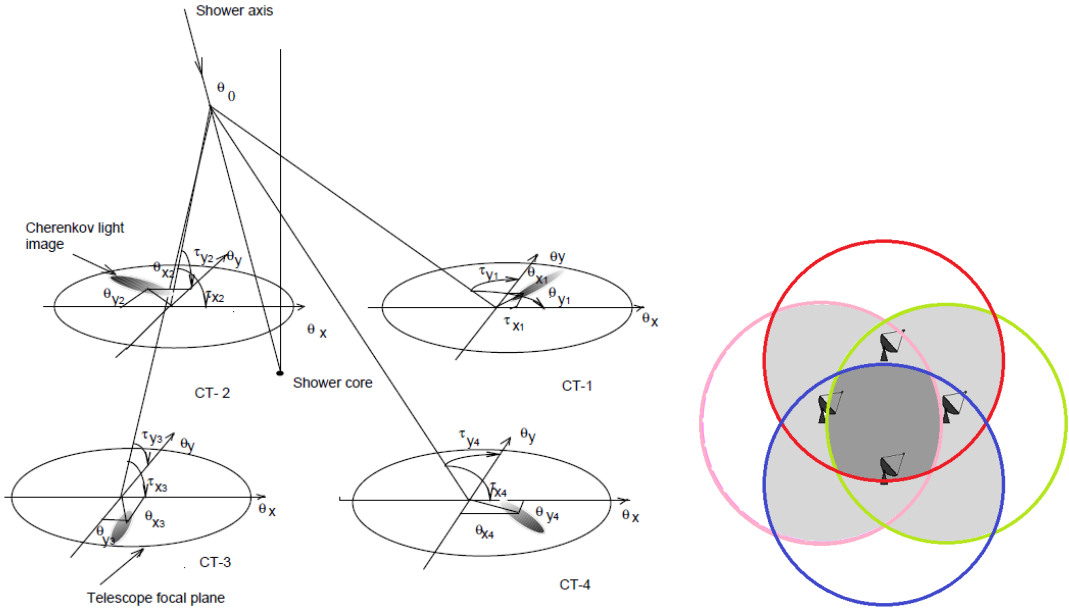
Another typical magnitude used to characterize and compare the performance of IACTs is their effective area. It is related to the flux of γ -rays and the number of detected events by means of equation 2.8.

$$\frac{N_{excess}}{\Delta t} = A_{ef} \cdot \phi \quad (2.8)$$

The effective area, is directly related to the sensitivity, and therefore it is energy dependent and includes not only the actual reflector area, but also the effects of many other technical parameters such as the optics or the trigger scheme. It is usually expressed in square meters, being a more intuitive parameter than the sensitivity to compare IACTs or different technical options.

2.2.4 Arrays of IACTs

Observing a γ -ray shower with more than one IACT at the same time allows using stereoscopy to reconstruct the shower in 3 dimensions [23],[24]. Compared to the monoscopic observations, stereoscopic data recording allows a precise three-dimensional determination of the shower maximum position and impact parameter, an effective Hillas parameter [19] extrapolation, a better energy resolution and a more stringent rejection of muons, hadrons and NSB, the latter rarely hitting two or more telescopes contemporaneously. Moreover, it also improves the angular resolution, making possible to distinguish sources which are very close.



(a) Shower image reconstruction with a stereo array of 4 IACTs [23] (b) Collection areas of an array of 4 IACTs [25]

Figure 2.14: Scheme of stereoscopic observation with an array of IACTs

Using an array of several IACTs decreases the effective area, because the number of events producing images in at least two telescopes is smaller, as shown in figure 2.14(b). However, due to the advantages of stereoscopy, much more background events are rejected, improving sensitivity. Nowadays, all currently active IACTs are part of arrays of telescopes which observe together.

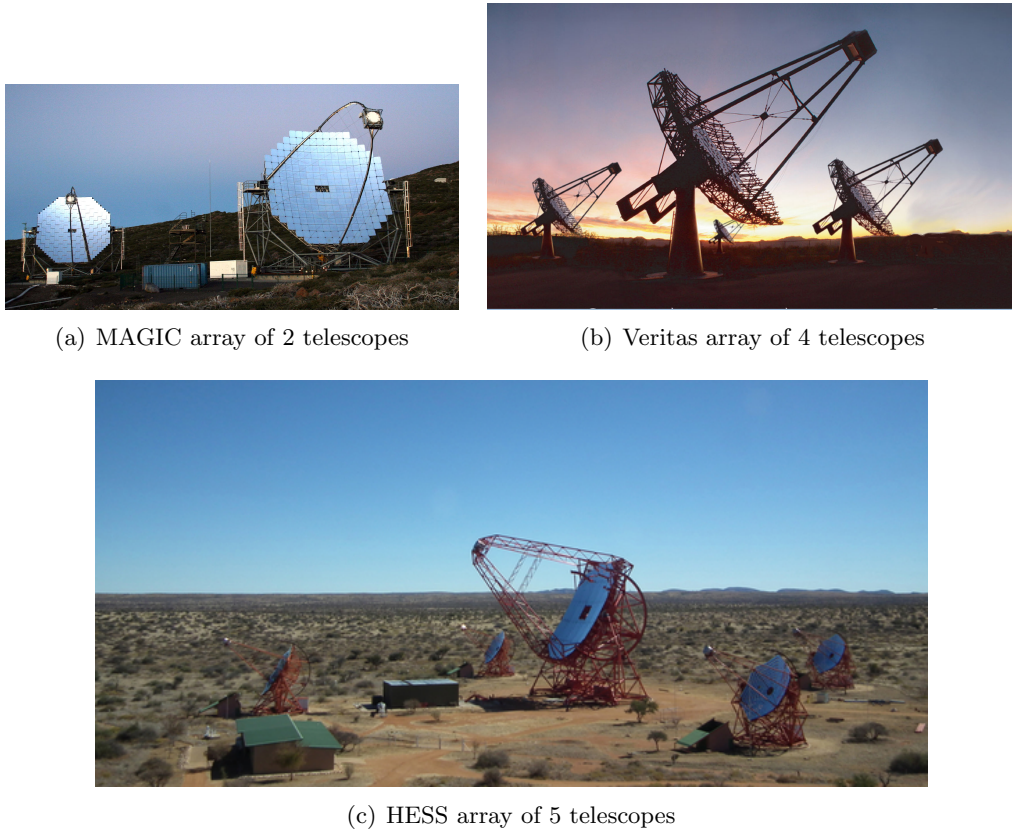


Figure 2.15: Currently active arrays of IACTs

2.2.5 Comparison between direct detection and Cherenkov technique

One can wonder which technique, the direct detection or the Cherenkov technique is more effective to detect γ -rays. The answer depends on the specific energy range under study. The higher the energy, the lower the flux of γ photons, according to figure 2.16. For this reason, the performance of satellites is limited for energies higher than 100 GeV. For instance, Fermi can only collect only 1 or 2 photons of these energies for a certain source every year. On the contrary, γ -rays with energies higher than 100 GeV cause large showers, with many Cherenkov photons which are easy to detect with IACTs.

On the other hand, the performance of IACTs is limited for energies lower than 50 GeV. At these energies the size of the Cherenkov showers is small, with not many Cherenkov photons. These characteristics make these showers difficult to distinguish from the night sky background photons and the showers originated by cosmic rays. In this way direct detection is preferable for low energies, while the Cherenkov technique is more effective for high energies. The highest part of the energy range detectable by Fermi slightly overlaps the lowest part of the energy range detectable by IACTs like MAGIC, as it is shown in figure 2.17. However, the performance of both satellites and IACTs between 10 GeV and 80 GeV is quite bad due to the fact that they are working near their limits.

One possible solution to improve the sensitivity in the energy gap between 10 and 80 GeV is to develop Cherenkov telescopes with large reflector areas, in order to detect as much Cherenkov

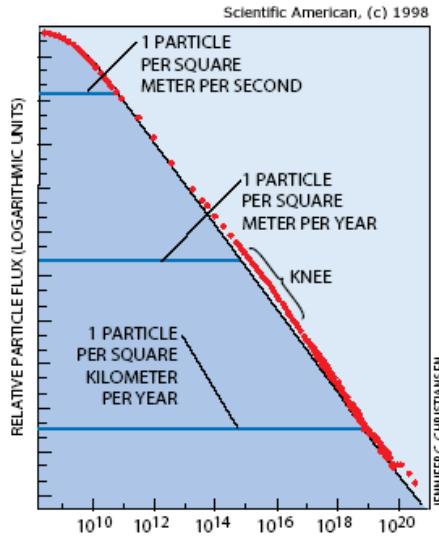


Figure 2.16: Relative particle flux vs energy. A similar behaviour can be observed for hadrons, muons and γ -rays

photons as possible and thus making possible to characterize γ -ray sources in this energy range. Additionally, energies from 100 GeV to 100 TeV are still of great physical interest, so that building new IACTs and improving the Cherenkov technique is also justified in order to improve the sensitivity in this “classical” IACT energy range. Better sensitivity means less observation hours required and, at the end, the possibility to analyze sources with lower γ -ray flux.

2.3 Imaging Atmospheric Cherenkov Telescopes

Several telescopes have been developed in the last 25 years making use of the Cherenkov technique explained in section 2.2.2. The first one was Whipple, which in 1989 detected a TeV emission from the Crab Nebulae for first time[27]. After Whipple, other IACTs were built like HEGRA [28][29] or CANGAROO [30] (already obsolete) and the currently active HESS [31] in Namibia, VERITAS [32] in Arizona and MAGIC [33] in the Canary island of La Palma. During the time they have been operational these telescopes have done important discoveries [34]- [37], becoming the main instruments to study γ -ray emissions above 50 GeV. The following subsections explains briefly several technical aspects of the IACTs, which define their characteristics and performance.

2.3.1 Mechanics

A Cherenkov telescope basically consists of a large reflector which collects the photons of the showers and reflects them into a camera. The larger the reflector the more photons that can be collected, which is specially critical to detect small showers generated by low energy γ -rays (lower than 100 GeV). For this reason important efforts have been done to build large IACTs. VERITAS telescopes are 12 m diameter, as well as HESS-I ones, MAGIC ones are 17 m and, HESS-II, which

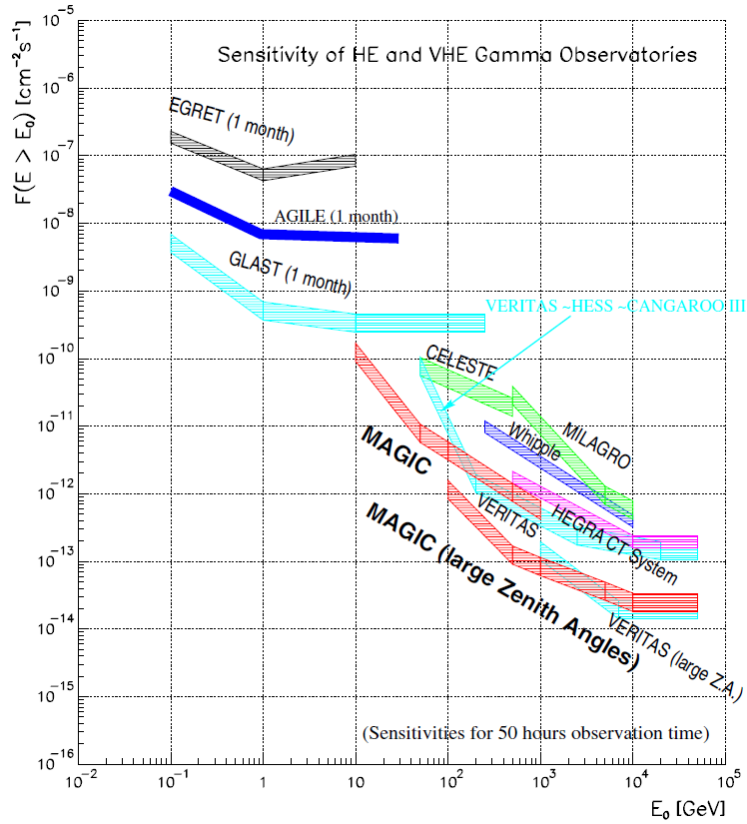


Figure 2.17: Comparison of integral sensitivities for ground based and satellite γ -ray experiments. The sensitivity is defined as the minimum flux of particles per square centimetre and second required to detect a source with a 5σ significance over the background after 50 hours observation for IACTs and 1 month for satellites [1],[26].

was still in its commissioning phase when this thesis was written, has a reflector with a diameter of 28 m.

To move accurately such a large structure both in azimuth and elevation is a delicate task. For instance HESS-II weighs 580 tonnes, and it requires 12 wheels in 6 bogies on a 36 m diameter rail and 4 servo motors to move in azimuth and other 4 motors to move in elevation [31]. In spite of them, it must be moved slowly because of the large inertia of the system. The movement of the telescope greatly simplifies if the structure of the telescope is made of carbon fiber tubes instead of steel, as it is done in MAGIC [38]. The price of the structure increases but it allows to move the telescope much faster, which is very useful to observe GRBs which can last only few minutes.

The main element of the optics of an IACT is its reflector. This reflector is not made by a single mirror (the price would be unaffordable), but composed of many individual tessellated spherical mirrors which can be reoriented by means of individual actuators like the one in figure 2.19. The reorientation of the mirrors is done periodically to maintain the optimal shape of the telescope reflector, compensating possible deformations of the structure due to gravity, wind, etc.

Besides its own weight and the mirrors, the structure must support the weight of the camera, which can be around 1 tonne and is usually hung from an arch or from a 4 masts structure. The design

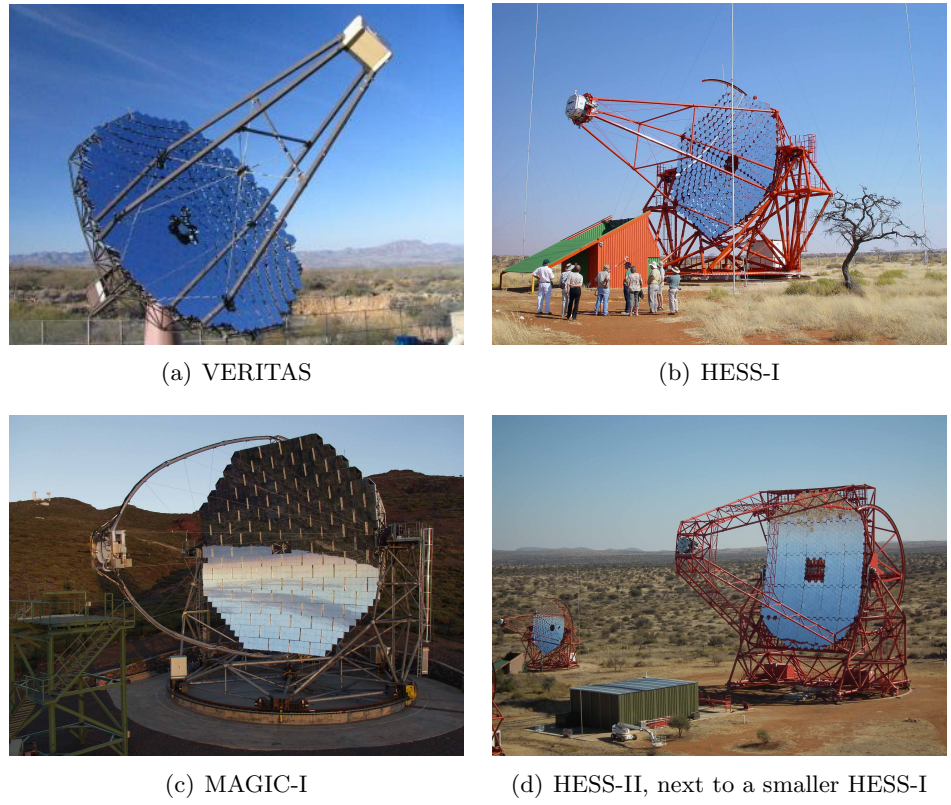


Figure 2.18: Some currently active Cherenkov telescopes

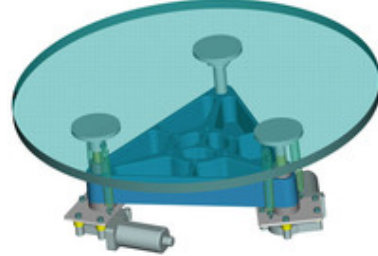


Figure 2.19: Scheme of one of the HESS mirror actuators [39]

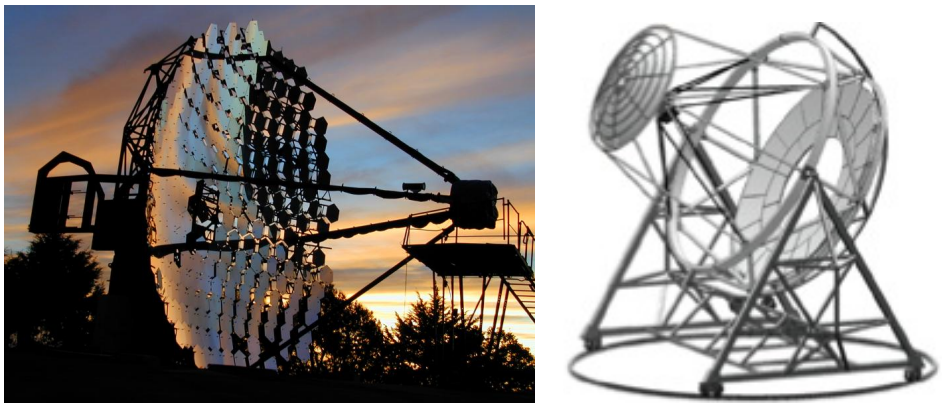
of this structure avoiding vibrations and deformations in every position is always a big challenge. Moreover, to let the telescope work safely, all the structure is designed to resist strict conditions of wind or even earthquakes.

2.3.2 Optics

The optics of the IACTs have several differences with respect to the ones of large optical telescopes. First of all, IACTs are not focused to infinity but to 10 km high in the atmosphere, where Cherenkov showers have their maximum. In this sense it can be said that a Cherenkov telescope is more similar to a photograph camera taking pictures of the extended air showers, than to a

traditional telescope.

Another important characteristic of the IACTs is that, as the Cherenkov showers last only few nanoseconds, it is important to ensure that the photons which were generated at the same time and travelled as a flat wavefront, arrive to the camera at the same time. This requires the use of tesselated parabolic reflectors with overall parabolic shape, so the length of the paths that the photons have to travel is the same. A Davies-Cotton design [40] instead of parabolic is also possible for IACTs designed to detect showers generated by γ -rays with energies above 100 GeV. This optics combine moderate time dispersion and larger fields of view (with smaller aberrations) than parabolic designs, being suitable for the slower and larger showers generated by the rays with higher energies [41]. Other optics based on double reflectors have also been proposed [42], but with no practical implementations up to now.



(a) Whipple telescope, with a Davis-Cotton optics made up of spherical mirrors (b) Proposal of IACT with double reflector

Figure 2.20: Different optical schemes suitable for IACTs

The mirrors which compose the reflector are not usually manufactured individually to form the required overall reflector shape, but they have a spherical shape (with different focal lengths depending on their distances to the reflector center) in order to save costs. The radius of curvature of this spherical shape is long enough to approximate accurately the focal length of the overall reflector shape once the mirrors have been placed on the structure. The mirrors are usually made of polished glass, aluminized and anodized. The thickness of the anodized layer determines the wavelength at which peak reflectivity of the mirror is obtained, so it is optimized for the wavelength range of the Cherenkov light. With this technique reflectivities higher than 90% can be obtained at the interesting wavelengths (300-600 nm).

Once the photons are reflected in the mirrors they arrive to the camera. As the photodetectors need some structure to be supported, it is not possible to cover all the focal plane with photodetectors. However, this potential loss of efficiency is solved by using Winston cones (as shown in figure 2.21) or lenses which collect all the light and lead it to the photosensors.

2.3.3 Photodetectors

The photodetectors used in IACTs must be very sensitive to detect the largest possible proportion of incoming photons. In this sense the Photon Detection Efficiency (PDE) is defined as the efficiency



(a) Winston cones of different sizes (b) A cluster of 7 pixels with Winston cones

Figure 2.21: Winston cones

to detect an incident photon and produce a current peak at the output of the photosensor. These detected photons are usually known as photoelectrons (pe).

At the same time the photodetectors must have a very short transit time to take advantage of the short development time of Cherenkov showers (a few nanoseconds), in order to avoid the accidental addition of Cherenkov and NSB photons. Taking into account a typical NSB-induced rate in each photodetector of a few hundreds of MHz, this means that the width of the output pulses can not be longer than few nanoseconds.

There are several photosensors which comply with the necessary requirements:

2.3.3.1 Photomultipliers

The photomultipliers (dubbed PMTs) are the photosensor most commonly used in IACTs. They consist of a photocathode, several dynodes and an anode, all enclosed in a vacuum tube, as it is shown in figure 2.22(a). When an optical photon of a certain wavelength range (optimized for the precise application) arrives to the photocathode, it extracts one electron due to photoelectric effect. This electron is accelerated towards the first dynode. When the electron hits this dynode, more electrons are generated by the process of secondary emission. Each dynode is set to a more positive voltage than the previous one, so the number of electrons in the beam is multiplied in each stage, until reaching the anode. Here, the electrons are taken out of the device forming a current pulse like the one in figure 2.25. The larger the number of dynodes and higher the voltage, the larger the amplification factor is, being possible to obtain up to 10^7 electrons for each impinging photon.

However, the PMTs have several limitations. Firstly, the electrons are not generated in the dynodes at the same time, but with a certain time dispersion which depends on the number of dynodes, the high voltage applied and other parameters. This limits the time resolution of the device, although it is worthy to mention that there is not any other kind of device with better time resolution. Secondly, PMTs sometimes generate their output pulses without any input photon or generate more than one pulse for the same photon, due to dark current and after-pulsing respectively. Dark current is produced by several reasons [43], but mainly by thermionic emission of electrons from the photocathode and dynode surfaces. Thus, the dark current rate gets increased with temperature and supply voltage. Regarding the afterpulses, they consist of spurious pulses which sometimes appear some time after the output pulse disturbing accurate measurements of low level signals, degrading energy resolution and causing error in photon counting. Most afterpulses appearing with

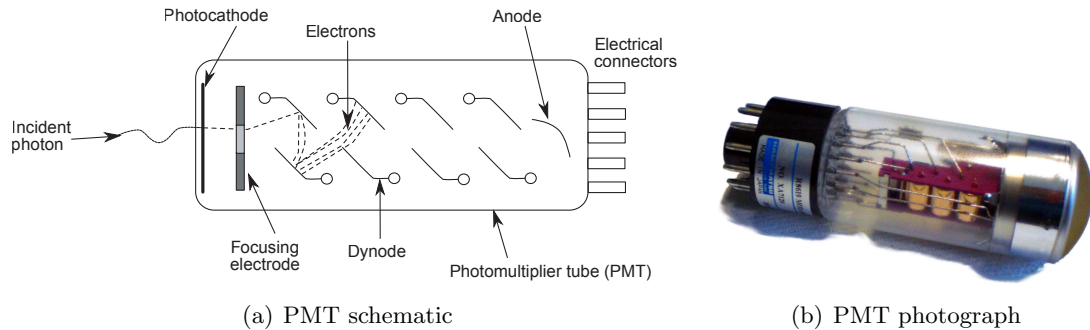


Figure 2.22: Photomultipliers

a delay of a few nanoseconds are caused by elastic scattering electrons on the first dynode or by sparks in the last dynodes generating photons which find the way back to the photocathode. On the other hand, afterpulses with longer delays (of the order of microseconds) are usually caused by the positive ions which are generated by the ionization of residual gases in the photomultiplier tube [43], [44]. Finally, the PMTs need to be manufactured by hand, being expensive for mass production.

2.3.3.2 Avalanche Photodiodes

APDs are the semiconductor equivalent to PMTs. The electron-hole pairs generated by photoelectric effect in the semiconductor p-n junction are accelerated by means of an intense electric field appearing in the dedicated semiconductor layout of the APDs. If the accelerated carriers have an energy high enough to ionize the atoms in the crystal lattice, more electrons and holes are generated which also contribute to the global current. These additional carriers are also accelerated, thus generating even more carriers and causing the avalanche [45], [44]. Typical values for the electric field required to produce the avalanche effect are around 10^5 V/cm for Si, corresponding to a 100-200 V reverse bias voltage. With these devices it is possible to obtain gains up to several hundred of electrons for each photon. This multiplication process, being not deterministic, introduce an excess noise due to the fact that the number of carriers generated in each avalanche is not the same. Additionally, APDs suffer other limitations. In order to increase their photon detection efficiency (the proportion of photons which trigger an avalanche), the devices must be thick and with a large area. However, this increases the transit times of the carriers and the capacitance, producing wider pulses and reducing the maximum operating speed. The dark current of these devices is also a limitation, requiring operation at low and controlled temperature to maintain it under reasonable values.

2.3.3.3 Silicon Photomultipliers

An strategy to increase the gain of APDs consists of increasing even more the reverse bias voltage above the APD breakdown voltage. In this situation, named “Geiger mode”, the internal electric field is so high that a gain around $10^5 - 10^6$ electrons per photon can be obtained. However, in Geiger mode the gain of an APD is not proportional to the incoming number of photons but a fixed large-amplitude pulse is associated to each group of incident photons, regardless its number. Such high current pulses would destroy the device, but this can be avoided connecting the APD to a quenching resistor. Based on this idea, a Silicon Photomultiplier (SiPM) consists of an array

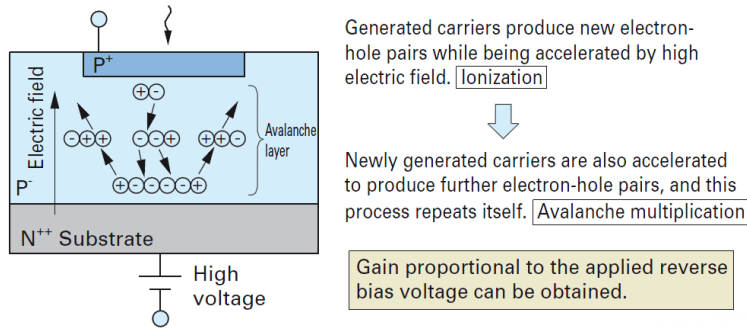


Figure 2.23: APD scheme

of APD cells operated in Geiger mode and with quenching resistors, as shown in figure 2.24(b)[46]. Being the area of each cell very small, for low light intensities the probability of having more than one photon impinging to the same cell is very reduced, so the sum of the outputs from each cell forms the SiPM output, which allows the photons to be counted (figures 2.24(c) and 2.24(d)).

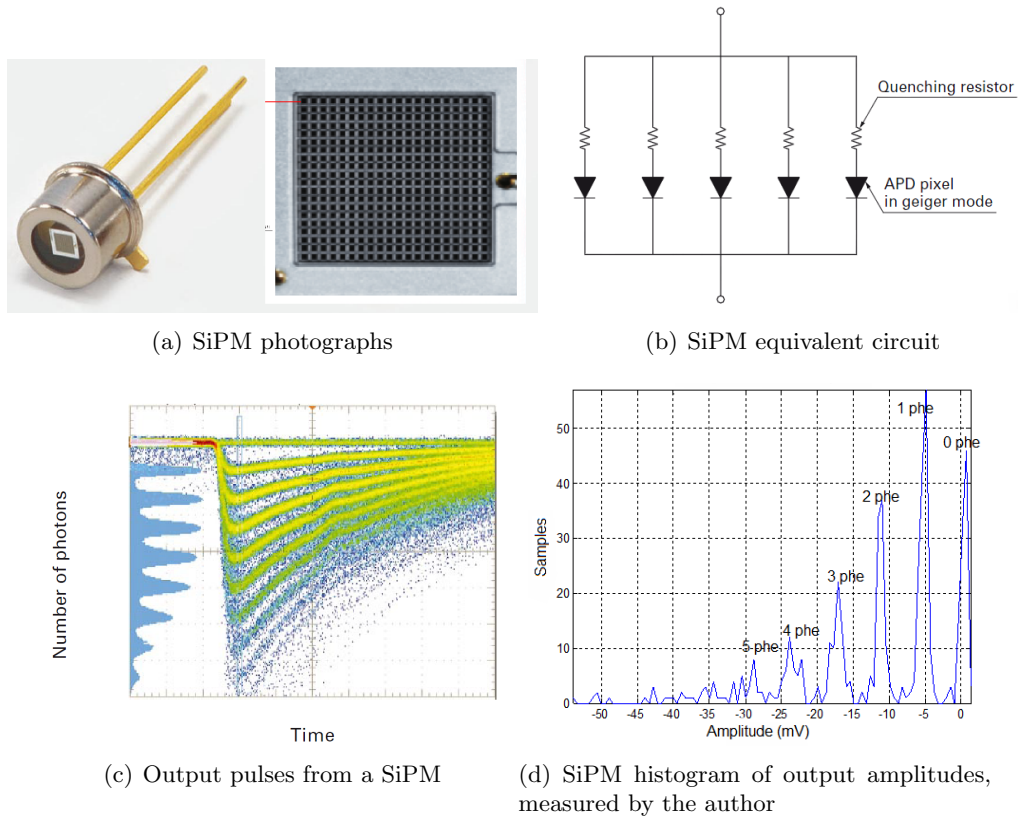


Figure 2.24: Silicon Photomultipliers

SiPMs have several advantages over PMTs. First they don't need bias voltages larger than 70 V, which makes them easier to handle. Second, they are not affected by magnetic fields, which has made them very popular in radiodiagnostic equipment embedded in high magnetic fields (like combined Positron-Emission-Tomography and magnetic resonance) and other medical applications.

In addition, they can reach a PDE higher than PMTs. And last but not least, although they are still rather expensive, they can get the best of the economy of scale of the Si technology, being possible to produce them very cheap [47]. Moreover, it is possible to integrate in the same chip the photosensors and their ancillary electronics [48].

Their main limitation is that, as well as for APDs, there is a trade-off between photon detection efficiency, the dynamic range and the speed of the device. SiPMs with large cells provide larger detection efficiencies, but their capacitance is higher and the pulses wider. With smaller cells it is possible to obtain shorter pulses and a larger dynamic range, but the gain and the efficiency is lower. Nevertheless, although some years ago the limitation in pulse width was important (see figure 2.25), the technology is advancing very fast and today there are SiPMs with short output pulses and a PDE similar or larger than the best PMTs. If the improvements continues, there is wide agreement that SiPMs will be the technology used in future IACTs. An IACT named FACT (First G-APD Cherenkov Telescope) [50], using SiPMs, has already been developed for R & D purposes.

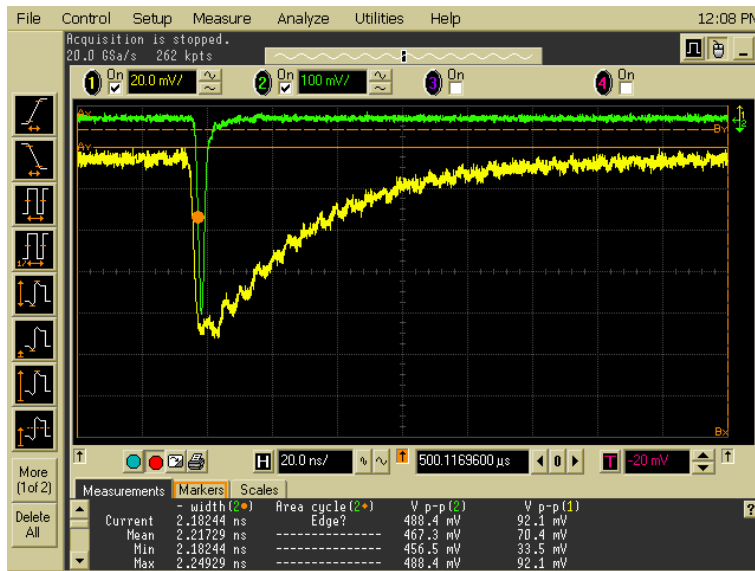


Figure 2.25: Output pulse produced by a PMT (green) and a SiPM (yellow) [49]

2.3.3.4 Hybrid Photodetectors

It is worth to mention another interesting device which combines PMTs and semiconductor technologies. A Hybrid Photodetector (HPD) consists of a semitransparent photocathode (like the PMT ones) and of an avalanche diode serving as amplification stage. When applying a several kV high voltage to the photocathode, the photoelectrons are accelerated in the high electric field and impinge onto the AD producing around 1000 electron-hole pairs. This is the so-called electron bombardment amplification. Those electrons subsequently induce avalanches in the active volume of the avalanche diode and provide an additional gain of around 100 when a bias voltage of a few hundred of volts is applied to the diode. Due to this high signal gain, HPDs have a very good amplitude resolution. Some attempts were done to use HPDs in Cherenkov telescopes [51], but their use has not been extended due to the difficulty to work with the very high voltages they need, ten times higher than for conventional PMTs.

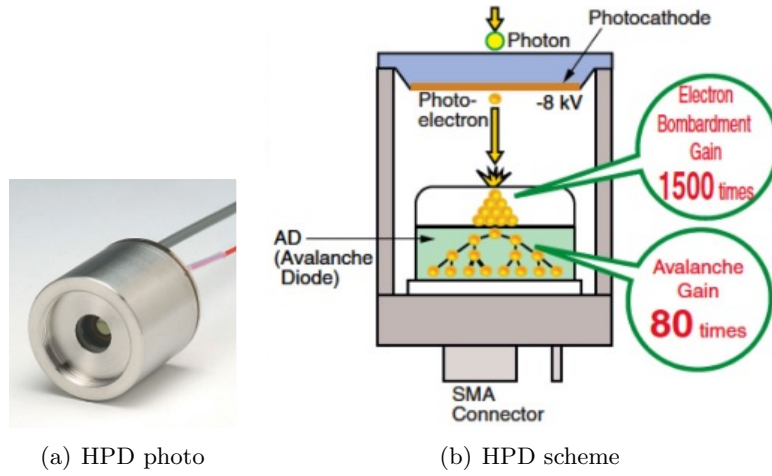


Figure 2.26: Hybrid photodetector

2.3.3.5 Photodetector comparison

Table 2.1 gathers the main characteristics of the photosensors commented in the previous sections. PMTs have been the prevailing technology since the first IACTs were built. APDs have a very good photodetection efficiency but the gain is too low to work with very low light intensities where photon counting is required. HPDs have a high gain and an acceptable PDE, but the very high voltages required complicate very much to work with them. Finally SiPMs combine a high gain and a good PDE, without requiring high bias voltages. As the SiPM technology is progressing, the limitations regarding pulse width or crosstalk are being overcome and the spread of this technology is expected to lower the prices. Once the SiPM technology will consolidate, it will likely replace the PMTs in the cameras.

Parameter	PMT	APD	SiPM	HPDs
PDE	35%	50%	55%	35%
Gain $\left(\frac{e^-}{photon} \right)$	$10^6 - 10^7$	100	$10^5 - 10^6$	$10^5 - 10^6$
Bias voltage (V)	≈ 1000	100 - 200	≈ 70	≈ 10000
Dark current	Yes	Yes	Yes	Yes
After pulsing	Yes	rarely	Yes	very rarely
Temperature influence	Medium	High	High	High
Price for mass production	Expensive	Cheap	Cheap	Expensive

Table 2.1: Comparison chart of the main kinds of photodetectors suitable for IACTs

2.3.4 Readout systems

The pulses generated by the photosensors (typically PMTs), being very narrow, need to be sampled very fast in order to determine with high precision its leading edge, and to integrate its charge in a narrow window which allows to reduce the noise contribution induced by NSB. A typical

2.5 ns width pulse from a PMT needs to be sampled at 800 MHz to recover at least the first lobe according to Nyquist theorem ⁴, being 1 Gs/s a typical sampling frequency. Considering that an IACT camera can have around 1000 pixels and 8 quantization levels, a continuous recording of the signals from all the pixels in a camera would mean a data rate of 1 TB/s, which is unmanageable.

The solution adopted in current IACTs [52] - [55] to have a reasonable amount of data is not to record continuously, but only when an interesting image appears. In order to do so, they use very fast analog ring memories [56],[57] capable of saving analog samples of the input signal voltage at a high sampling rate. These memories are used as a buffer: when a new sample is taken, it is saved in the place of the oldest one. So, the buffer always contains the last samples of the signal. In parallel to the readout system, the analog signals from the pixels also feed a trigger system which analyzes the inputs and decides if there is an interesting image in the camera or not. If the trigger system decides that the image deserves to be stored, it orders the readout to stop sampling and then the signals present in the analog memories are digitized. Finally, these digitized samples are formatted adding timestamps, event numbers, all the rest of information regarding the status of the telescope and the atmospheric conditions, and stored to disk.

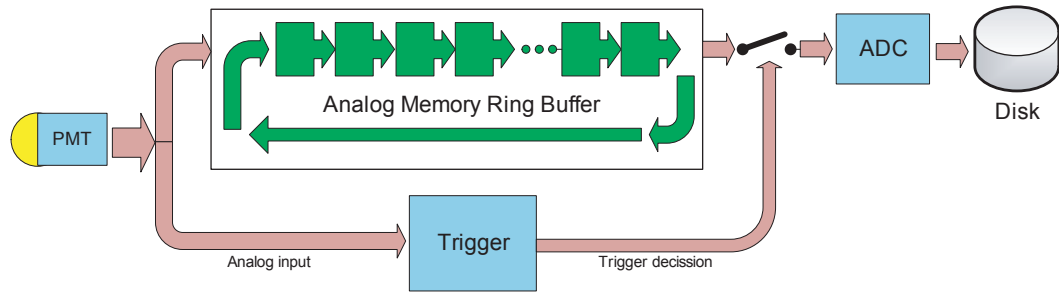


Figure 2.27: Scheme of a readout based on analog memories

The number of samples stored in the analog buffer must be large enough to allow the trigger system do the required operations to decide whether the event is interesting or not. Longer buffers allow more complex trigger schemes which lead to a better NSB rejection as will be shown in the following chapters of this thesis. The length of the buffer and how the other functions are performed depends strongly on the particular implementation of the readout. For instance, in the readout used in MAGIC [52], [53], the Domino Ring Sampler (DRS [56]) chips are used as analog memories with a buffer length of up to 1024 cells, while the digitization of the samples is done in commercial ADCs and the samples are directly stored. On the other hand, in the readout implemented for HESS-II the analog memories are implemented with a specially designed ASIC named Swift Analogue Memory (SAM [57]) with a buffer length of 128 cells. In this case the digitization is also done in commercial ADCs but, after that, the integrated charge of the digitized signal is calculated and only the charge and the arrival time of the pulses are stored instead of the samples, reducing the amount of data recorded to disk. More recent schemes aimed to provide readout systems for the next generation of IACTs are in its development phase. In this way NECTAr [58] has integrated a 1024 cells analog memories and the ADCs in a single ASIC to improve reliability and cost, while the DRAGON [59] project has developed a readout system with 4096 cells by cascading 4 DRS4 chips in order to increase the buffer length up to 4 μ s and thus allow a more complex trigger system.

⁴In fact it can be sampled somewhat slower because the PMT pulses are not square but “gaussian”.

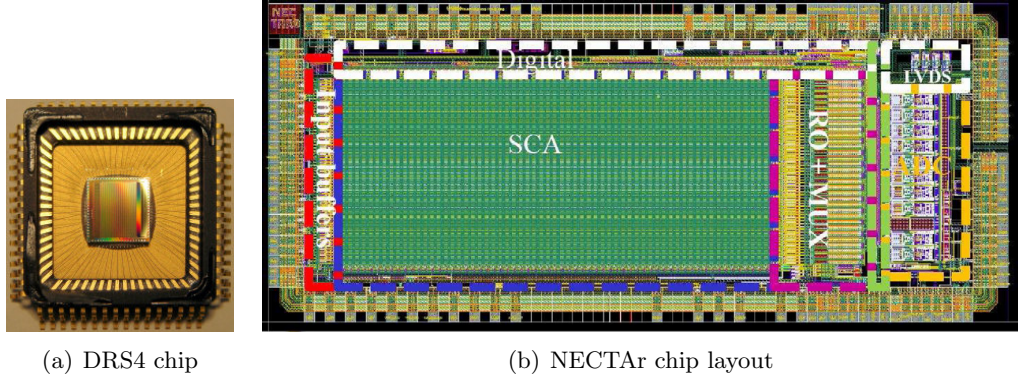


Figure 2.28: DRS4 and NECTAr chips

Readout	Cells	Digitization	Stored data
MAGIC	1024	In commercial ADC	Samples
HESS-II	128	In commercial ADC	Charge and arrival time
NECTAr	1024	Integrated in chip	Charge and arrival time
DRAGON	4096	In commercial ADC	Samples

Table 2.2: Characteristics of several readout schemes based on analog memories

However, the readout systems based on analog memories have an intrinsic limitation. When the signals in the buffer are being digitized there are not samples being saved in the analog memories, so the possible events appearing during this time are lost. This is why this time is known as “dead time” and must be reduced as much as possible in order to get the best telescope performance. The dead time can be reduced in two ways: improving the speed of the digitizers or reducing the number of samples which must be digitized. There is not much to do regarding the first option but waiting for the industry to develop faster ADCs at a reasonable price for c.a. 2000 channels per camera. However, it is possible to reduce the number of samples to be digitized. This does not mean to have shorter buffers but to know, with great accuracy when the trigger happened. In this way, digitizing a time window of a few tens of nanoseconds around the trigger time will be enough to save the interesting samples.

A different readout strategy recently proposed and without the dead time limitation consist of using wider pulses (by using photosensors producing wider pulses or slow filtering the narrow ones generated in a PMT), digitizing them continuously at a lower frequency (typically 80 MS/s) and, from the digital samples, decide if these samples must be stored or not [60]. This idea, being already possible, is not suitable for observing Cherenkov showers generated by low or medium energy γ -rays (10 GeV - 1 TeV) in a context of high NSB. In this case, the intensity of the light from the showers (and therefore the amplitude of the digitized signals) is comparable with the one from the NSB. If the pulses are wider, maybe 5 or 6 ns, the probability of overlapping the pulses coming from the shower and the NSB is increasingly high, and the resulting integrated charge will include both signal (Cherenkov) and background (NSB) photons, distorting the data recorded. However, for higher energy showers, typically above 1 TeV, with very large Cherenkov pulses per image pixel, it is a rising option.

2.3.5 Data management

In spite of recording only triggered events, IACTs still collect large amounts of data, specially if there are several telescopes working in stereoscopic mode. For instance, MAGIC-I and MAGIC-II produce around 1.5 TB of raw data every night. To manage and process such amount of information, a powerful computing infrastructure is required. In order to manage the data efficiently and optimize the bandwidth usage between the different processing stages, the data is usually processed in several steps. For example, for the MAGIC telescopes case, a first real time analysis [61] takes place in the counting house, looking for anomalies and triggering alarms if a problem is detected or a transient cosmic source shows a high emission state. Once the observations of the night are finished, an analysis of the data is performed at the telescope site [62], with the aim to check if the data events are properly constructed, analyze the quality of the data, compress them in a clever way and transform the data in a more manageable format. After this first analysis, the data is usually sent to a data center [63]-[65] where they are finally stored and deeply analyzed by means of supercomputers or grid networks. Telescope sites are usually in remote places, far away from the large data centers and with a limited connectivity, so it is important to compress the data before sending them. In addition, a good backup policy is required. Sometimes there are more than one data center, in different continents, offering data and computing services to the global scientific community.

2.3.6 Auxiliary systems

The main elements of a Cherenkov telescope have been introduced in the previous sections. However, there are other auxiliary systems which are also necessary for the operation of the IACTs. They are briefly mentioned in the following subsections:

2.3.6.1 Timing

All the recorded samples must be synchronized and all the events must be timestamped accurately. This is essential to observe objects with temporal variation like pulsars or GRBs, or to study objects at different wavelengths in coordination with other telescopes working at different frequencies. Therefore, an accurate timing system is required to generate the timing signal which must be stored together with the data. This is usually solved with Rubidium or Cesium clocks disciplined by GPS to correct possible long term variations. These systems provide an accuracy better than 30 ns with respect to UTC with great stability. Although this is out of the main topic of this thesis, it is worth to mention the contribution of the author to the timing system currently working at the MAGIC site [66] [67].



Figure 2.29: Rubidium clock synchronized by GPS, model Symmetricom XLI, like the one used in MAGIC

2.3.6.2 Pointing

IACTs need to be pointed very accurately to distinguish the real origin of the γ -rays. In other wavelengths there is always a visible light peak coming from the source, so fine pointing can be done with no more than adjusting this light point in the middle of the photosensor. However, the objects producing γ -rays are usually quite dark at other wavelengths because they are not linked to thermal reactions and, besides that, the camera is not focused to infinite. The solution is to place a CCD in the center of the dish and see the surrounding stars which are reflected into the camera, adjusting the image to the expected one. These pointing corrections must be applied both while the telescope is tracking a source in the sky and later on when γ -ray showers are reconstructed and analyzed [68], [69].

2.3.6.3 Calibration

In a complex system like a Cherenkov telescope, there are many parameters whose variation can influence the global response. Therefore, some systems need to be calibrated frequently to correct these variations. For instance, the pointing of the individual mirrors need to be readjusted with their actuators to correct the effect of wind and gravity in different positions. This can be done by placing a laser in the center of each mirror and pointing it to the center of the camera, with the lids closed, serving as a screen. A CCD camera at the center of the reflector checks if all the laser spots are focused in the center of the camera, or the position of some mirror needs to be corrected [70], [71].

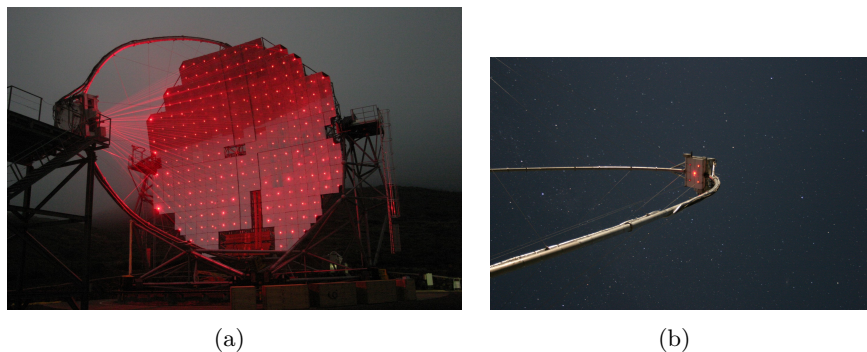


Figure 2.30: MAGIC mirror pointing calibration

Other important calibration is the equalization of the gains of the camera PMTs. In spite of using photomultipliers of the same model, they might provide different gains for the same high voltage and this distorts the measurements. To correct this effect, some lasers or LEDS are placed in the center of the reflector, focused in such a way that they illuminate the whole camera with nearly the same light intensity. These light sources will generate short flashes, mimicking the few nanoseconds Cherenkov pulses. Measuring the amplitude of the outputs, it is possible to adjust the high voltage of the individual PMTs equalizing the gain of the different channels [72]. At the same time, changing the bias voltages of the PMTs change their transit times introducing delay inaccuracies which also need to be calibrated, as will be described in chapter 6.

2.3.6.4 Cooling

The photosensors and the analog amplifiers present in the camera are sensible to temperature variations, so a camera cooling system is required to stabilize it. This has been solved in different ways. In the MAGIC telescopes a water cooling circuit is used, which provides a very fine temperature control [73]. However, it is also heavy, complicating the mechanics of the arch. In HESS or VERITAS it is done simply with blowing air with fans, which is a much lighter solution but not so accurate [74]. The best cooling system depends on the sensitivity of the precise components, the amount of power dissipated in the camera and the outside temperature.

2.3.6.5 Weather conditions and security

IACTs are installed in places where the weather conditions are good enough to observe most of the time. However, there are always limits in the weather conditions beyond which observations can not take place. For this reason, there is always a weather station and different sensors near the telescope, which are directly connected to several security systems. For instance, it must not be possible to switch on the PMTs during the day, because they would be burned. In the same way, over a certain wind speed, the telescope must be fixed in the parking position. As most of the photosensors use high voltages, additional care must be taken with humidity to avoid sparks or electric shocks to the operators, etc. It is worth mentioning that IACTs can not be protected with domes like in the case of optical telescopes, because the large reflectors required by the former would need prohibitive large and expensive domes.

2.4 The Cherenkov Telescope Array

Current systems of Cherenkov telescopes use at most five telescopes, providing best stereo imaging of particle cascades over a very limited area, with most cascades viewed by only two or three telescopes. An array of many tens of telescopes would allow the detection of γ -ray induced showers over a large area on the ground, increasing the number of detected γ -rays dramatically, while at the same time providing a larger number of views of each shower. This would result in both improved angular resolution and better suppression of cosmic-ray background events. With the aim of building such array of IACTs, the Cherenkov Telescope Array (CTA) Consortium was created [75]. Today, more than 1000 people in institutions of 27 countries (see figure 2.32 work together to make it a reality, being one of the future large research infrastructures included in the European Strategy Forum on Research Infrastructures (ESFRI) roadmap [76], and a recommended project for the next decade by the US National Academies of Science [77].

The CTA Consortium aims to build two observatories in both hemispheres with tens of telescopes in each one. With a budget of around 200.000.000€ the installation of the first telescope prototypes in the sites is schedule at the beginning of 2015, while the installation of the majority of the telescopes will take place in 2016. There will be three types of telescopes with different reflector sizes, optimized to cover different energy regimes [2], [78]. They are explained in the following subsections:

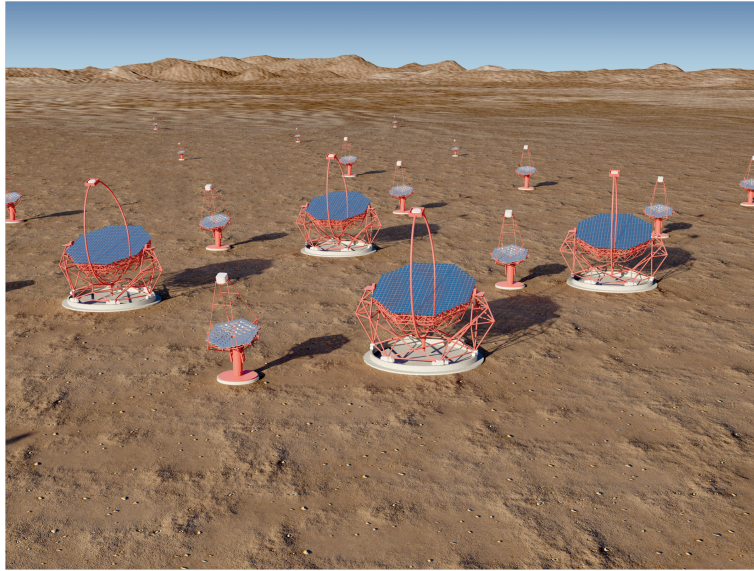


Figure 2.31: CTA concept

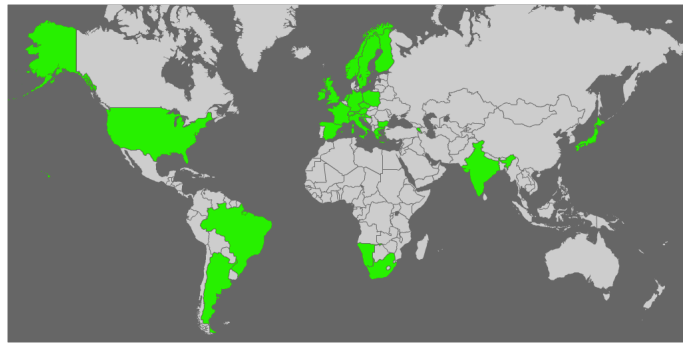


Figure 2.32: Countries participating in the CTA Consortium

2.4.1 Small Sized Telescopes

The small-sized telescopes (SSTs) will be optimized to detect showers generated by γ -rays of more than few TeV and up to 100 TeV. In this high energy range the flux of γ -rays is severely reduced, as was shown in figure 2.16, so a large area in the ground must be covered to increment the number of detected showers. In this way, a high number of SSTs is required, covering an area of several square kilometers. Additionally, well above the SST energy threshold, the Cherenkov showers are very large and with many photons, so if the shower is in the field of view of the telescope, it is very easy to collect enough photons to reconstruct it. Due to these characteristics of the showers generated by γ -rays above several TeV, the SSTs will have relatively small reflectors (4-6 m diameter) and a field of view of around 10° . Moreover, as the telescopes need to be cheap (to build many of them) and a very high sensitivity is not required, the SSTs are the ideal place to use innovative designs based on double reflector optics⁵, or SiPMs (see 2.3.3.3).

⁵After two reflections, a certain amount of photons are lost. For this reason, this kind of optical schemes are not recommended to detect showers with few photons

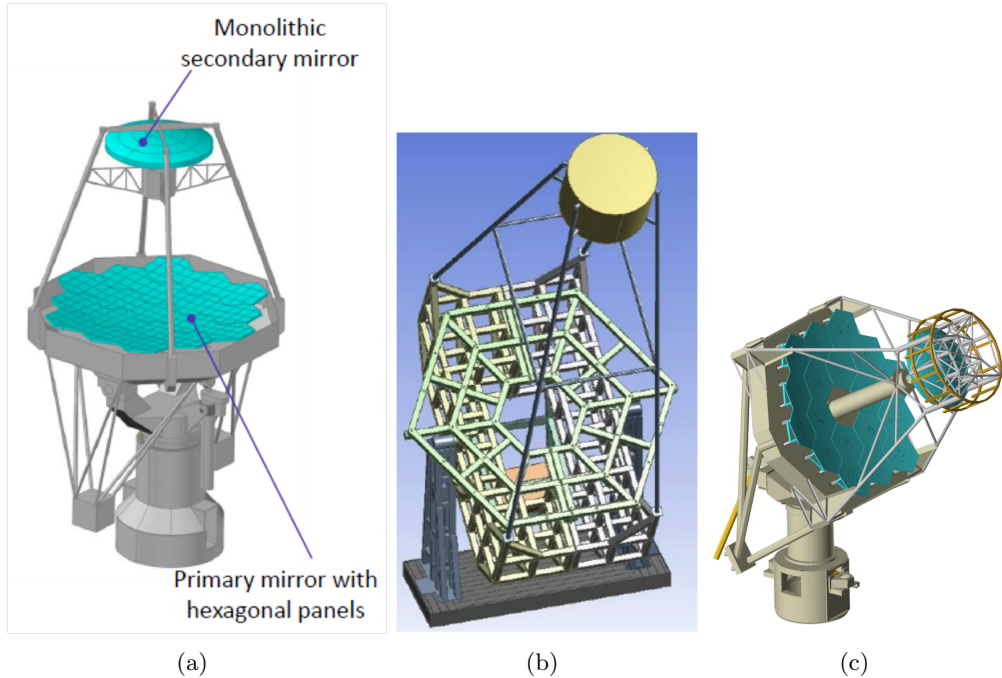


Figure 2.33: Some design concepts for the SSTs

2.4.2 Medium Sized Telescopes

Medium-sized telescopes (MSTs) will be optimized for the medium energy range, from 100 GeV to 10 TeV. The coverage of this energy regime is instrumental for the CTA project, as the 100 GeV - 10 TeV range includes a large fraction of the cosmic objects to be discovered and studied by the ground-based γ -ray astronomy in the next 20 years. This is the typical energy range covered by current instruments and, based on them, the MSTs will have a reflector of around 12 m and a field of view of 6-8 degrees. The main improvement in sensitivity of CTA in this energy range will come from the large area covered, and from the higher quality of shower reconstruction, since showers will be typically imaged by a larger number of telescopes than for current few-telescope arrays (see section 2.2.4).

2.4.3 Large Sized Telescopes

The large sized telescopes (LSTs [79]) are aimed to detect γ -rays between 10 GeV and 100 GeV, covering the relatively unexplored energy gap between the maximum energy γ -rays detectable with satellites and the minimum energy ones detectable with current IACTs. This is a very interesting energy range because the Fermi satellite has already detected around 2000 sources, while current IACTs can only observe less than ca.100. Therefore, unknown mechanism are taken place in the cosmic sources to *switch them off*, precisely in this energy regime. At these energies the showers are small and very faint, so telescopes with large reflectors (23 m diameter) are required. The best optical performance of the telescope is achieved with focal lengths similar to the reflector diameter. This imposes a restriction on the camera weight and size, and therefore small fields of view (around 5°) are enforced. Moreover, improving the sensitivity to low-energy γ -ray showers is a big challenge

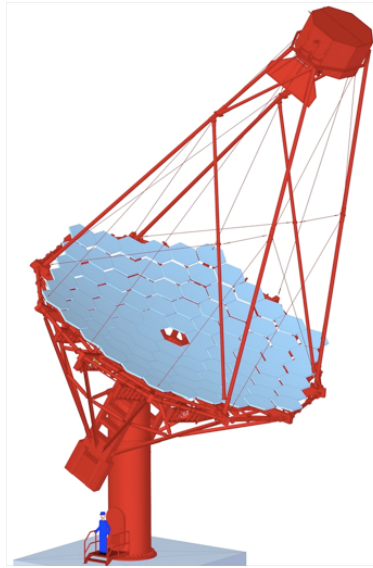


Figure 2.34: Design concept for the MSTs

for the photosensors, which must have a high PDE, the readout, which must be able to sample very fast adding low electronics noise, and for the trigger system which needs to distinguish between NSB and signals which have approximately the same intensity.

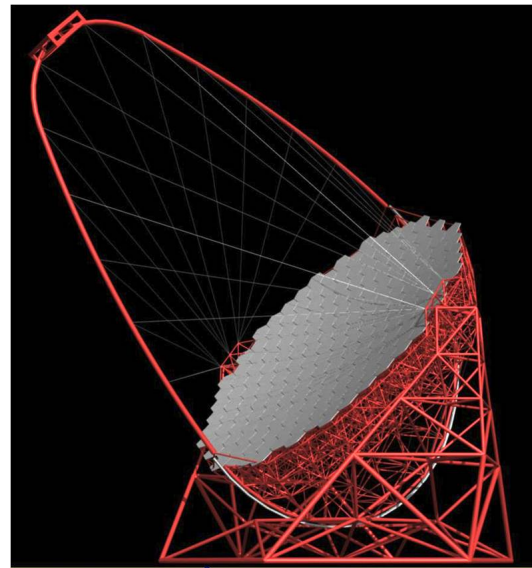


Figure 2.35: Design concept for the LSTs

2.4.4 Expected Sensitivity

In the current status of the design phase, CTA observatories will count with 4 LSTs, at least 30 MSTs and between 35 and 70 SSTs depending on the funds availability. The global performance

of the array for the different energy ranges depends on the position, amount and properties of the different IACTs, so in order to find an optimal configuration many Monte Carlo simulation studies have been performed [80]. According to these simulations array E in figure 2.36 seems to be the most balanced option for the full CTA energy range. With the three types of telescopes working together, the global sensitivity of the array is improved as it is shown in figure 2.37(a), achieving better sensitivity and angular resolution than current IACTs (figures 2.37(b) and 2.37(c)). With this expected performance it will be possible to obtain a deeper knowledge of all the γ -ray emitting objects already mentioned in section 2.1 [81], [82].

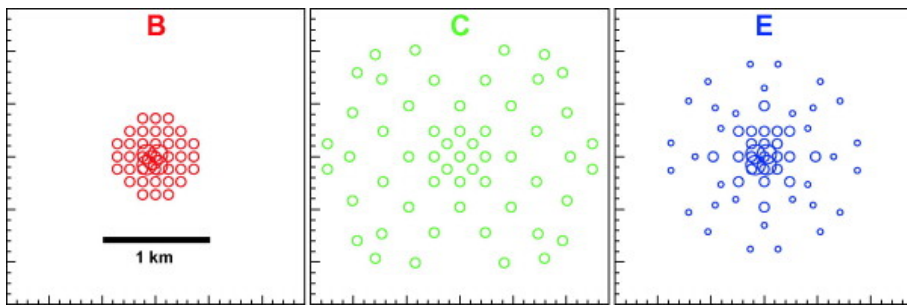
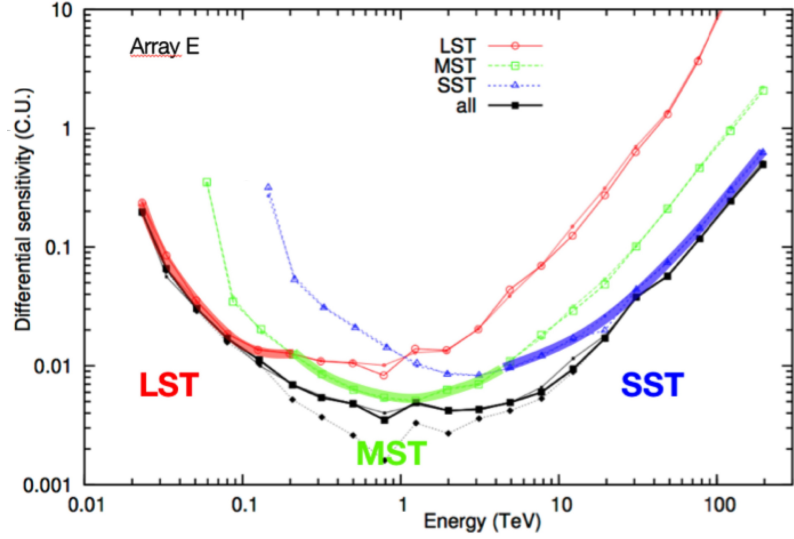
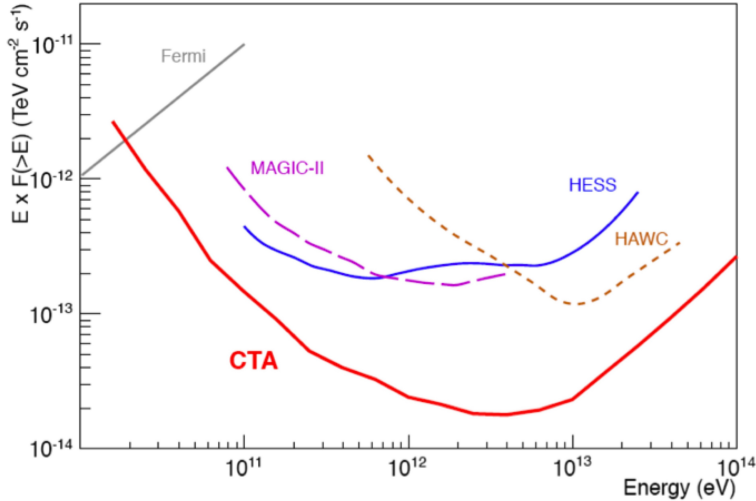


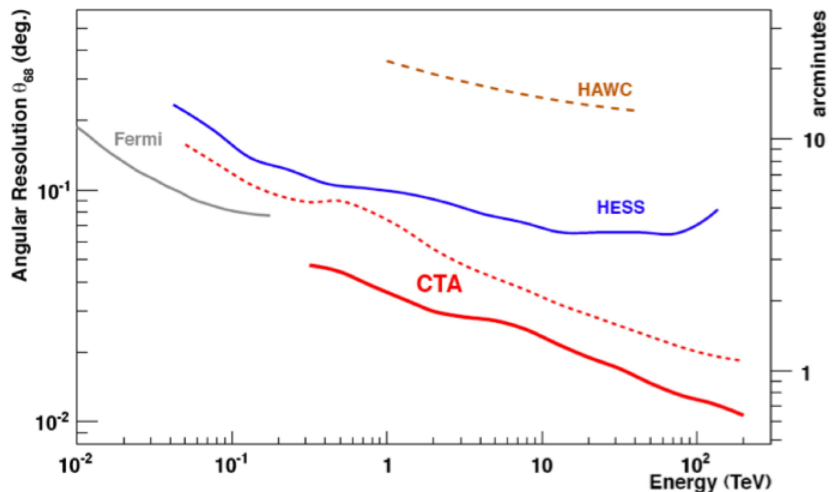
Figure 2.36: Different possible array layouts. According to simulations, the most balanced performance is achieved by array E.



(a) CTA expected differential sensitivity, in units of the energy-dependent flux of the Crab nebula, for 5σ significance after 50 hours of observation



(b) CTA expected integral sensitivity compared with other γ -ray observatories, in light flux, for 5σ significance after 50 hours of observation



(c) CTA expected angular resolution, compared with other γ -ray observatories, for 5σ significance after 50 hours of observation

Figure 2.37: CTA expected performance for array E [2].

Chapter 3

The Trigger System.

As was previously introduced in section 2.3.4, most of the data acquisition systems currently used in IACTs consist of analog memories which sample very fast the analog pulses coming from the photosensors. These samples are not digitized continuously, but only when the trigger system detects that they correspond to an interesting Cherenkov shower. So, the main function of a trigger system is to distinguish between gamma-like images and those originated by background. However, it is not easy to define what an interesting image is. Most of the IACTs are triggered whenever a certain number of close pixels detect a number of photons at a correlated time. This trigger condition is effective to reject most of the NSB-induced images, but the images corresponding to isolated muons or hadrons are also recorded (see fig. 3.1) and the events should be classified as gammas or hadrons in a further step, by means of image analysis software. With the aim of speeding up this analysis, some trigger schemes implement real time image pattern recognition systems, which are able to reject also hadrons. The problem of such systems is that, for Cherenkov showers caused by low energy gamma rays (20-80 GeV), it is very difficult to distinguish gammas and hadrons in a simple way. The image projected by a low energy γ -ray is a short ellipse, which resembles the image projected by a low energy hadron.

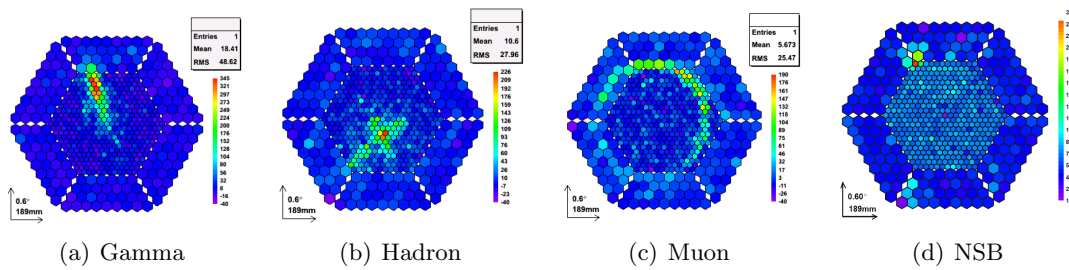


Figure 3.1: Recorded images for different kinds of events and NSB [10], [11]. The different colors indicate the amount of light collected by the pixels.

Apart from recognizing simple image patterns in order to discard NSB-induced images, the trigger system must comply with several requirements in order to work together with the readout electronics. First, the trigger decision must be taken and distributed to all camera clusters in a short time (known as latency), which is limited by the length of the analog buffer. In fact, the length of the buffer is designed to be long enough to let the trigger decision be taken properly. The longer the

buffer, the more expensive the readout is, so the trigger must be as fast as possible to reduce cost. Nevertheless, if stereoscopy is used, a buffer of at least several hundreds of nanoseconds is required to receive the trigger information from telescope neighbours which can be 100 m away or even more.

Another parameter which must be minimized is the jitter. When the readout is triggered, it digitizes a few tens of analog samples around the time in which the trigger was produced. For instance, if the trigger needs 800 ns to take the decision and distribute it to the readout of all the channels, the readout will digitize several samples around the one which was taken 800 ns before. If the trigger system needs a different amount of time to be generated and reach the readout for each event (jitter), the length of the window which must be digitized should be increased accordingly, thus requiring more time to digitize each event and increasing the dead time of the system. Moreover, in some analog memories sampling systems like DRS4 [56], the different memory cells are not completely homogeneous, introducing a slightly different gain factor depending on the cell which contains the precise sample. These gain variations can be calibrated only if the numbers of the cells which contain the information are known, and this knowledge is only possible if the jitter of the trigger system is very low.

The dead time of the readout determines the maximum trigger rate that can be achieved by a telescope. If the trigger system triggers at a higher rate than the maximum one supported by the readout, some triggers will be ignored and their corresponding events will be lost. If this happens, the trigger condition (usually a minimal amount of light collected in a close area during a short time) must be tighten, so that only showers with larger signals fulfil the trigger condition, thus reducing the rate. Showers caused by low energy γ -rays are faint and appear at a larger rate than high energy showers. Therefore, the trigger must work with weak conditions and the highest rate allowed by the readout to detect them.

Summarizing we can say that, from a functional point of view, a good trigger system is one which is able to impose an intelligent trigger condition which can be fulfilled by Cherenkov showers (even by the weaker ones) but not by NSB, requires the shortest possible latency and introduces the smallest possible jitter, thus not contributing to increment dead time. In this way the telescope works at its highest possible trigger rate, with the maximum probability of detecting Cherenkov showers while rejecting NSB. With the aim of developing such a trigger system, multi-level trigger schemes are typically used.

3.1 Multi-level trigger basis

All trigger schemes are based on the fact that the photons generated by Cherenkov showers are collected by close pixels in a time window of few nanoseconds for the low energy primaries or few tens of nanoseconds for the showers caused by high energy γ -rays or hadrons. On the contrary, the photons of NSB impinge the camera in an uncorrelated way, following a Poisson probability distribution. This difference is used by the trigger systems in current IACTs, which look for coincident photon detections at different levels [83], [84], [85]. The following subsections describe a typical multi-level state-of-the-art trigger architecture.

3.1.1 Pixel level

The pixel level receives the signal directly from the pixels. The input from each pixel is compared with a threshold corresponding to a certain number of photoelectrons. If the threshold is exceeded, this level generates a logic “1” during a time which depends on the specific implementation, otherwise produces a “0”. So, this level can be considered to be looking for a pulse of Cherenkov photons in a single pixel. The outputs of several pixel level triggers feed the higher trigger levels.

3.1.2 Camera level

The camera level receives the inputs from the pixel level and decides if the image present in the camera corresponds to an image which deserves to be saved or not. Depending on the complexity of the algorithm and how it deals with the hadron showers images, it is possible to distinguish two types of camera triggers:

3.1.2.1 Trigger-region based camera triggers

3.1.2.1.1 Majority

The simpler camera trigger systems add the outputs of the pixel level corresponding to a certain number of pixels in a close region (usually called cluster or simply trigger region) and compares the addition with a threshold. If there are more than a certain number of pixels fired in the trigger region, the threshold is exceeded and the camera trigger is fired. As the NSB photons reach the pixels randomly, the probability of several pixels being triggered by NSB at the same time is low, so this technique is quite effective to recognize the Cherenkov photons, while rejecting the NSB. The optimal size of the trigger region depends on the energy of the observed γ -rays, the specific optics, field of view, etc. Current trigger regions in HESS contain 64 pixels [83] while in MAGIC they contain only 37, as shown in figure 3.2. Additionally some camera trigger systems impose that the fired pixels must be next neighbours, reducing even more the probability of being triggered by NSB [84], [85]. As the Cherenkov shower image can appear anywhere in the camera, the overlapping of the trigger regions is essential in order to detect the showers at any place.

3.1.2.1.2 Sumtrigger

The architecture described is the most common one and it is usually called “majority” trigger, because it generates camera triggers whenever a majority of pixels (above a given number) in a trigger region have a signal larger than a fixed number of photoelectrons (figure 3.3(a)). The limitation of this scheme comes from the fact that the amount of photons collected by the pixels is not taken into account for the decision. For instance, if a pixel has collected 3 photons and the threshold has been set to 4 photons, the three photons will not contribute to the trigger decision at all. On the contrary, if the output of a pixel exceeds the threshold, it does not matter if it collected just the minimum photons to exceed the threshold or several more ones. This limitation affects specially to the detection of weak showers from low energy γ -rays, which might not produce enough Cherenkov photons to fire enough pixels in any trigger region.

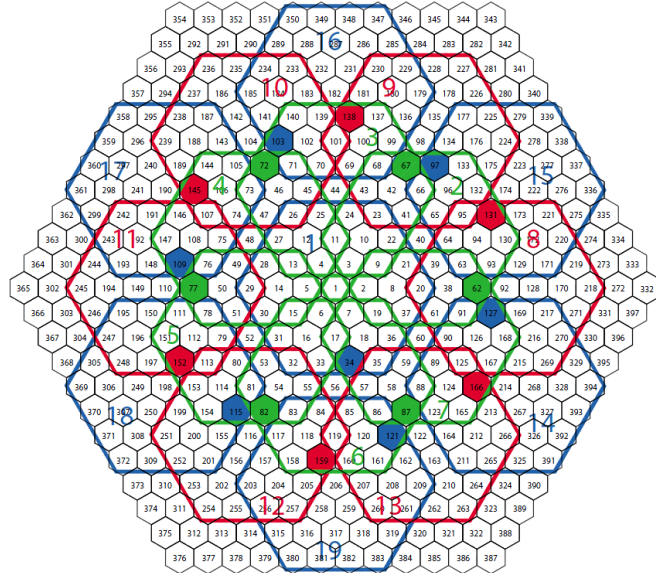


Figure 3.2: Level 1 MAGIC trigger regions [85]. In the figure only the inner pixels are shown, because the external ones do not participate in the original trigger scheme

A different trigger scheme was designed for first time to improve the sensitivity of the MAGIC-I telescope [86]. It is known as Sum trigger and consists of removing the comparators in the pixel level for overlapping trigger regions and send the analog inputs from the pixels directly (after properly conditioning) to the camera level trigger. The camera level performs the analog addition of the inputs from the pixels in every trigger region and compares the sum with a threshold (figure 3.3(b)). Thus, in the case of Sum trigger, the threshold does not correspond to a number of pixels, but to a certain number of photoelectrons collected in the trigger region. In this way, all the collected photons are taken into account, improving the sensitivity to weak showers.

Figure 3.4 shows the Montecarlo-expected improvement observed in the effective collection area of the old MAGIC-I telescope due to the use of the sum trigger scheme. The lower the energy of the γ -ray, the lower the number of Cherenkov photons that arrive to the camera and therefore, the number of showers which can be reconstructed. In the collection area plots like the one in figure 3.4, this reduction in the number of detected showers is represented as a reduction in the effective collection area. In the same way, it can be seen that the use of the sum trigger allows to detect more low energy showers, which is equivalent to have a larger collection area for that energy range.

The main problem of the sum trigger is how to deal with the afterpulses introduced by the PMTs (see section 2.3.3.1). The afterpulses caused by positive ions generated by the ionization of residual gases, taking place up to several μs after the main pulse, can have large amplitudes equivalent to 100 photoelectrons (phe) or even more, which would fire the sum trigger even if no more pixels have signal. In order to avoid these fake detections, the sum trigger needs a clipping circuit before the adding stage to limit the maximum pulse amplitude coming from each pixel. In figure 3.5 it can be seen how a clipping value corresponding to 6 phe in each pixel strongly reduce the number of triggers due to afterpulses, thus allowing to use lower threshold values with still manageable trigger rates, and therefore incrementing the sensitivity for low energy γ -ray originated showers.

The sum trigger increments the sensitivity in the low energy range but this is not for free.

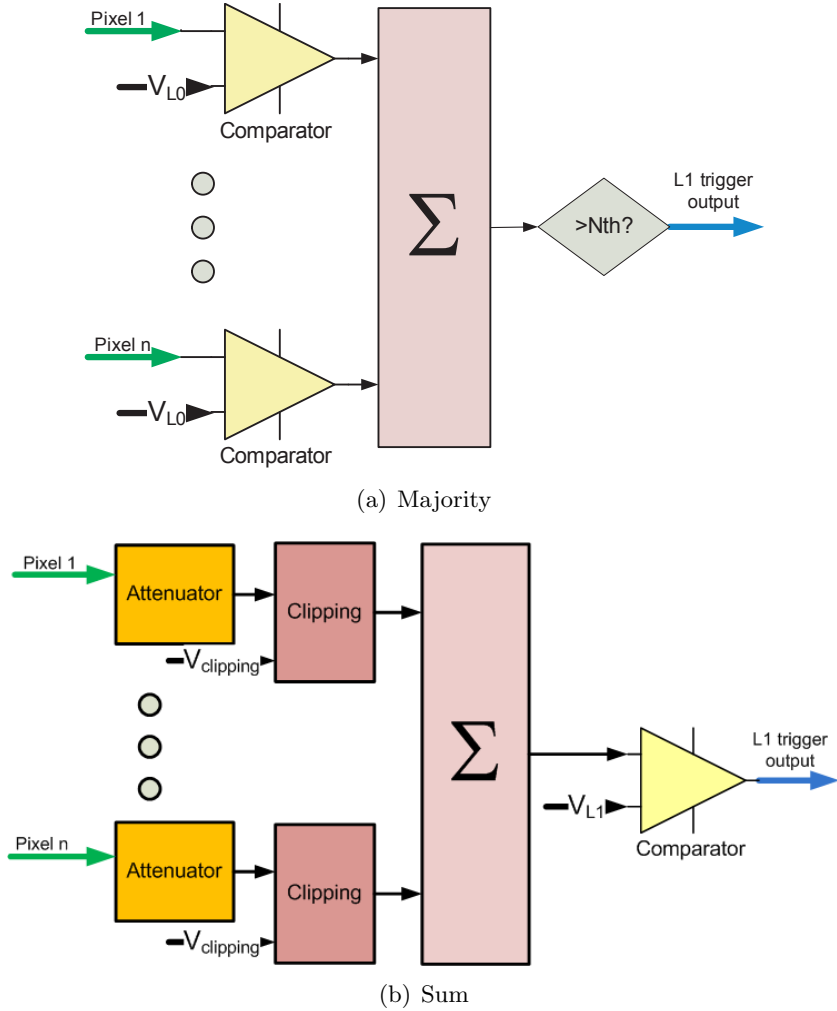


Figure 3.3: Generic schemes of the majority and sum trigger

Implementing the sum trigger scheme implies managing analog short pulses with high bandwidth, which need to be scaled, clipped, replicated (the same pixel can participate in more than one sum due to trigger region overlapping), and added analogically. All the inputs must go through all the stages at exactly the same time to add the signals properly, and the added noise from all the inputs should be low enough to distinguish individual photoelectrons. For these reasons, the development of sum trigger schemes is much more complicated than managing the digital signals in the majority trigger concept.

3.1.2.2 Pattern-recognition based camera triggers

More sophisticated camera trigger systems use the information from all the pixel level triggers in the camera and try to find patterns in the fast reconstructed images. In this way, this kind of trigger systems do not only distinguish between Cherenkov events and NSB, but they can also classify the Cherenkov showers as corresponding to γ -rays, hadrons or muons and, depending on the implementation, the hadrons and muons can be discarded or stored separately [87]. In order

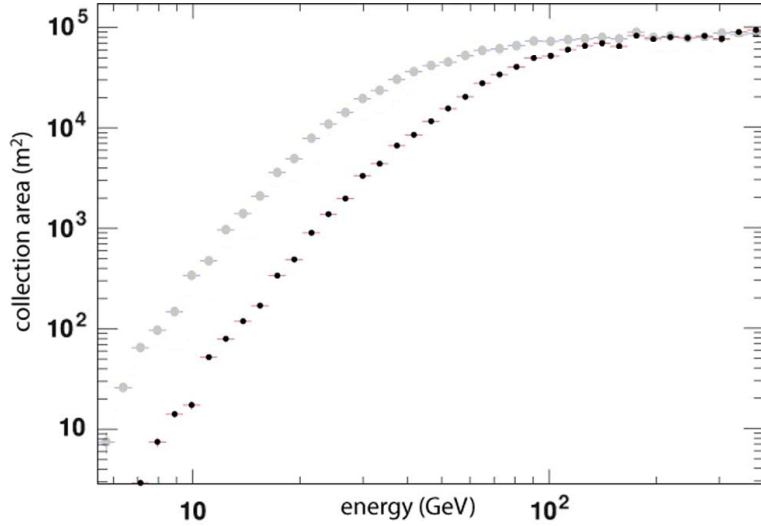


Figure 3.4: Collection area of the MAGIC-1 telescope with standard next-neighbour majority trigger (black dots) and sum trigger (grey dots)[86]

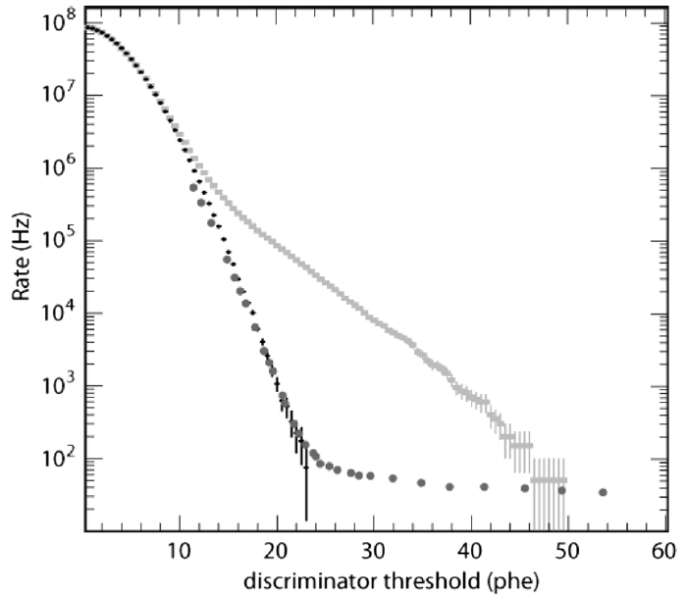


Figure 3.5: Trigger rate versus discriminator threshold of a MAGIC-I sum trigger region with clipping (black crosses and dark grey dots) and without it (light grey dots). The black crosses and the light grey dots represent rates obtained by means of Montecarlo simulations, while the dark grey dots correspond to rate measurements. For thresholds lower than 21 phe the NSB dominates, while for very high thresholds the rate is dominated by the cosmic-rays. In the middle thresholds is where the clipping effect is crucial.

to take the trigger decision in a short time, this kind of camera trigger algorithms run on fast digital electronics implemented with FPGAs and LUTs [85], [89], [90], considering the input from every pixel as a “0” or a “1”. As a consequence, these camera trigger algorithms work with very

rough information, so it is very difficult to get a good γ -hadron separation for low energy γ -rays. If the IACT is devoted to low energy observations, it is preferable to store on disk all γ -like events (as identified by a simple camera trigger algorithm) and afterwards to analyze the digitized data in a further step, running complex classification algorithms (usually based on machine learning techniques [91]) over the acquired image. The images provided by the acquisition system are richer in information, containing how many photons were collected in each pixel and their arrival time instead of only a “0” or a “1”. This is why these complex camera trigger algorithms based on pattern recognition have not meant a major progress in IACT technology and their utility is currently called into question.

3.1.3 Array level

When there are several IACTs working in coincidence in an array, it is possible to improve the NSB rejection by imposing that only the events which caused trigger in two or more telescopes in a given time window are digitized. The system which checks this condition is generally known as array-level trigger or “Stereo trigger” and is usually implemented as an electronic module in a central position of the array, as shown in figure 3.6 for the HESS telescopes. Every time that the camera trigger of one telescope is generated, it sends a trigger signal to the central unit, typically through an optical fiber. The array-level trigger looks for telescope triggers happening inside a time window of several tens of nanoseconds (typically 50 ns) and, if the trigger condition is satisfied, it sends the final trigger to the IACTs, which distribute the command to their clusters and pixels to digitize the event.

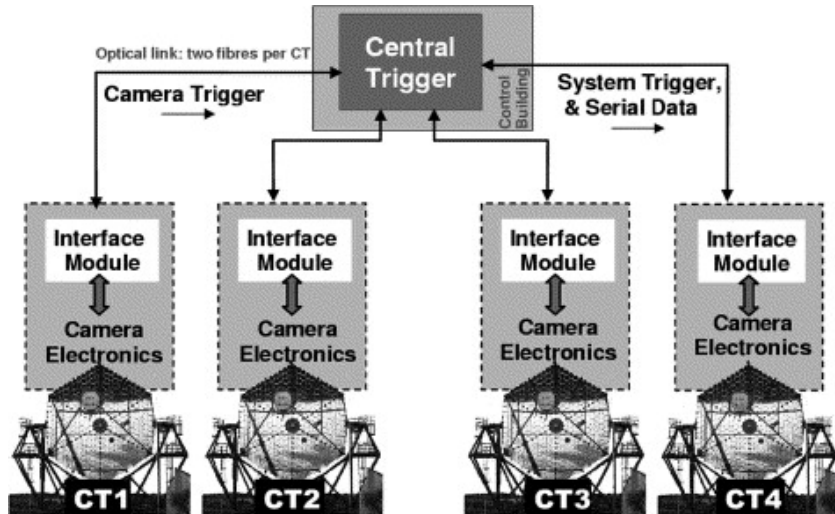


Figure 3.6: Scheme of the HESS array trigger [83]

The coincidence window between telescopes in this level is much longer than the coincidence window between pixels in a camera because the light impinging the different telescopes follows different paths in the air that, even after theoretical delay correction, introduce a physical jitter of up to a few tens of nanoseconds. This fact, together with the delay required to send the trigger signal from the telescopes to the central unit and back, makes necessary to have a minimum buffer of around 1 μ s in the pixel readout memories. Considering 50 m between the telescopes and the

central unit, 500 ns are required only for light propagation through the optical fibers¹. The longer the buffer the more expensive the readout, but a certain cost is acceptable, given the improvement obtained by the stereo trigger. The array-level trigger rejects most of NSB events, thus allowing to lower the thresholds in the pixel and camera trigger levels, and so incrementing the sensitivity to low energy γ -rays.

3.2 An Analog Trigger System for CTA LSTs and MSTs

The best trigger scheme to be installed in the CTA telescopes will depend on many parameters: the observed source, the sky brightness conditions, the moon, the site, the size of the telescopes, the optics, the PMTs, the electronics, the trigger architecture, etc. as well as also other technical parameters like the cost, the reliability or the power consumption which must be taken into account. In order to deal with so many parameters and being able to compare the performance of different trigger approaches proposed by different groups in CTA, several Monte Carlo simulations have been performed. In fact, there is a CTA working group fully devoted to perform Monte Carlo simulations which take into account most of the specific details of the CTA telescopes. This is the only way available to compare different trigger schemes which will be installed in telescopes which still do not exist, trying to simulate realistic conditions. Low level technical trigger parameters such as gain, latency, noise or bandwidth are not useful to compare different trigger schemes which follow different approaches and can be optimized to work in different conditions or to detect showers induced by γ -rays of different energies.

In this way, the target of the LSTs is to detect Cherenkov showers generated by γ -rays with an energy as low as possible and, in order to do so, a sum trigger scheme is expected to be the best alternative as explained in section 3.1.2.1.2. With the aim to confirm this assumption, several simulations have been performed, of which results in terms of collection areas are shown in figure 3.7 [93]. This figure compares the collection areas obtained with several trigger approaches, normalized by the one obtained with an analog sum trigger scheme adding 14 pixels² (*SumDoubl*, red line). The other schemes simulated have been the analog sum trigger of 7 pixels (*SumSingl*, grey dotted line), a combination of majorities (*OR(Maj3, Maj4)*, yellow dashed line), two digital implementations of sum trigger schemes with trigger regions of 14 and 7 pixels (*FlashCamDoubl* green dashed line and *FlashCamSingl* grey dashed line respectively), and a variation of a majority scheme which looks for 3 pixels fired in each group of 7, considering that the 7-pixel trigger region can be centered in any pixel in the camera (*ScSglMaj3*, blue dashed line). The digital implementations of the sum trigger follow a novel readout philosophy already mentioned in section 2.3.4: the analog signals coming from the pixels are sampled and digitized continuously at a frequency around 80 MS/s and the trigger sums the digital samples in fast FPGAs [60],[94]. In this way, it is possible to avoid working with analog signals. However, as it is shown in figure 3.7, the effective collection area can be around 40% lower than with analog sum trigger for low energies, due to the pulse stretching produced by the low sampling frequency.

On the other hand, the target of the MSTs is to build reliable and cost-efficient telescopes optimized to detect γ -rays between 100 GeV and 10 TeV, so the sum trigger is only preferable if it

¹considering 2×10^8 as the speed of light in the fiber and the round trip

²Each CTA cluster will contain 7 pixels, as will be explained in the following sections. These is why the simulated trigger regions always contain multiples of 7 pixels.

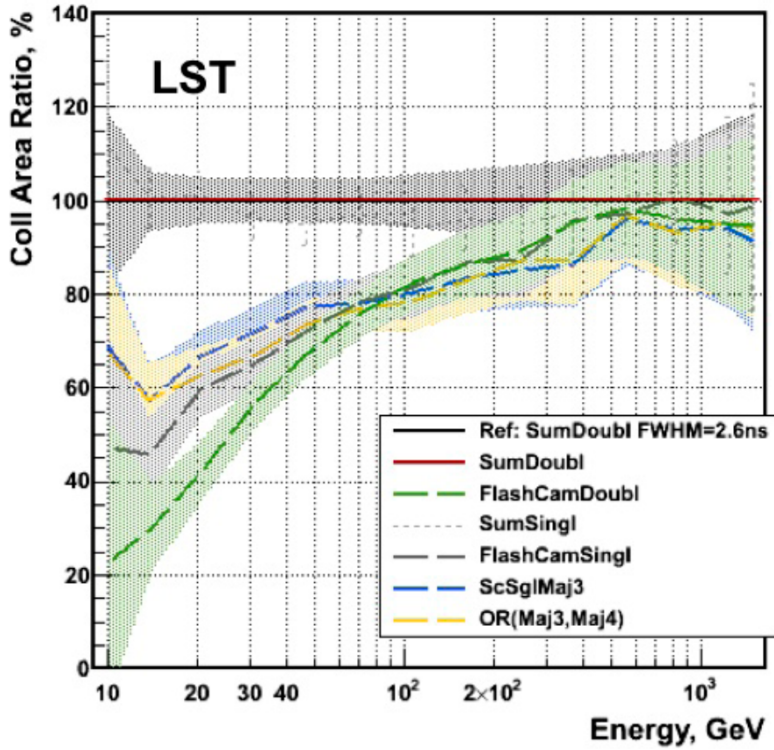


Figure 3.7: Simulated collection areas for different trigger schemes in CTA LSTs [93].

does not incur in additional costs. Simulations corresponding to MSTs are shown in figure 3.8 for the same trigger schemes described for the case of LSTs. The results show more similar performances between the different approaches than in the case of LSTs, with a slight advantage of the sum trigger in the lower energy range. In the medium energy range some digital triggers work slightly better than sum trigger and, when looking for high energy γ -ray showers, the digital schemes are clearly better. Nevertheless, the error bars are larger for higher energies, so these results should be accepted with some scepticism.

The author of this thesis, together with other members of the GAE-UCM group and other Spanish CTA teams at IFAE and Ciemat, have developed an analog trigger system, able to implement the sum trigger scheme. This trigger system is intended to be used in CTA LSTs, optimizing the sensitivity to the low energy showers, as expected from simulations of figure 3.7. Nevertheless, as the sum trigger scheme shows an acceptable performance in the middle energy range, and the cameras of CTA LSTs and MSTs are very similar, we have designed the trigger system to be also suitable for MSTs, optimizing costs and reliability. The trigger system consist of a multilevel scheme including from the pixel level to the array level as were defined in section 3.1, and designed to be compatible with all the electric and mechanical constrains of both LSTs and MSTs.

In the next section the hardware architecture of the LST and MST cameras is sketched, with the aim to make possible to describe the trigger developed by the Spanish groups in the following sections, as well as explaining the relation between the trigger and the other systems in LSTs and MSTs.

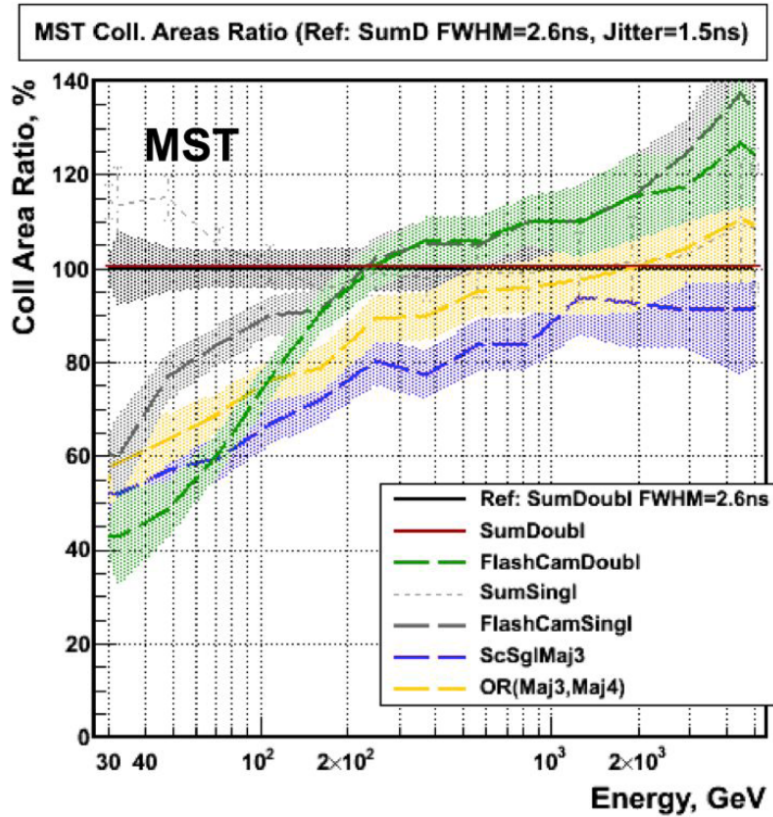


Figure 3.8: Simulated collection areas for different trigger schemes in CTA MSTs [93].

3.2.1 Camera hardware architecture

The camera architecture in LSTs and MSTs is very similar. Both cameras will have the same mechanical structure and cooling system, and this determines the number, size and positions of the different hardware elements. The camera pixels are grouped into hexagonal clusters of 7 pixels looking for modularity. To be precise, every camera will have 265 clusters of 7 pixels each, corresponding to 1855 pixels. The clusters are composed of several boards which will be described in the following subsections, and all of them are connected to the central camera systems, by means of direct cable connections or through the backplane network. These camera systems are in turn connected to a central array unit, which receives the digitized data and controls certain issues of the whole CTA.

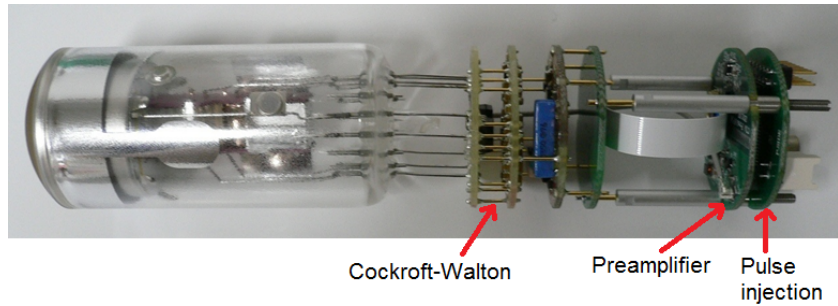
3.2.1.1 Pixel electronics

Every pixel has associated electronics as shown in figure 3.9, implementing the following functions:

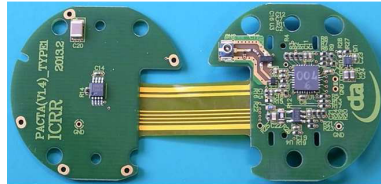
- Providing high voltage power supplies to the PMTs from a +24V DC general power supply. This is usually done by means of a Cockcroft-Walton multiplier.

- Preamplifying the output pulses from the PMTs and transforming the signal into differential to protect it from noise. In CTA LSTs and MSTs this is done with an ASIC named PACTA [95], specially designed for this work by a research group at ICC-UB.
- Pulse injection. These circuits can introduce an “artificial” pulse instead of the one generated by the PMTs, in order to test the electronics chain without operating the PMT with an optical light source.

The different electronic subsystems implementing these functionalities have been developed by Hamamatsu (the PMT manufacturer) and several Japanese groups, in the case of LSTs, and by the LAPP French group in the case of MSTs. In both cases the PACTA chip developed at ICC-UB is used for the amplification.



(a) Photomultiplier with its associated boards



(b) Preamplifier and pulse injection boards

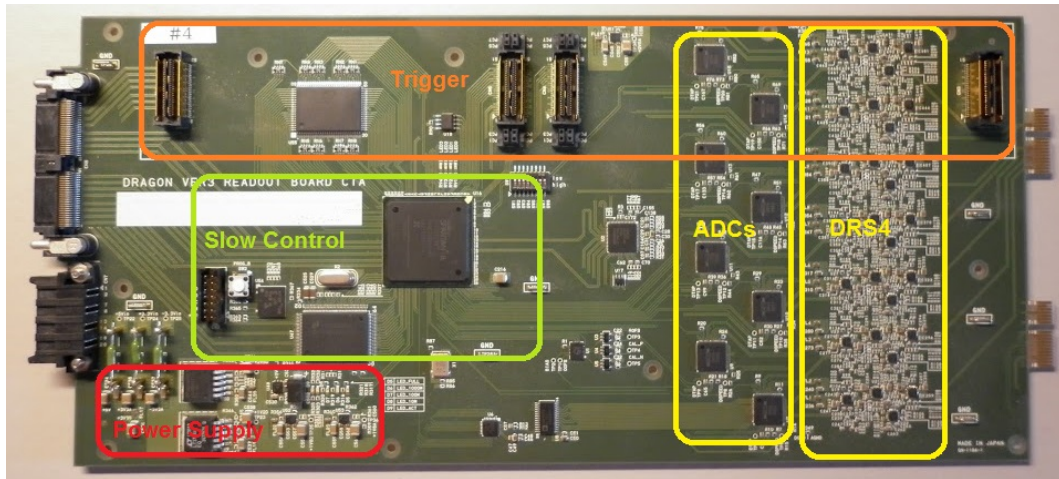
Figure 3.9: PMT and its associated electronics for LST

3.2.1.2 Front-end boards

The front-end electronics is the core of every cluster and is implemented in a single board. Each front-end board receives the 7 input signals from the pixels, adapting and replicating them to feed the readout and the trigger subsystems which are housed in this board (in the case of the trigger, only partially). The front-end board contains an FPGA which is in charge of the slow control functionalities, the data packet construction, and the transmission of the data and the slow control commands through an Ethernet interface. Additionally, the front-end boards contain a power supply system to obtain the different voltages required by the electronics from the general +24 V power supply.

The front-end board to be used in LSTs is named Dragon[59][96] (figure 3.10(a), developed by several Japanese institutes), while the one to be used in MSTs is known as NECTAr[58][97] (figure

3.10(b), developed by several french groups). Dragon is optimized to have a large buffer of $4 \mu\text{s}$, obtained by cascading 4 DRS4 analog sampling chips with $1 \mu\text{s}$ buffer each one. In this way, the buffer is long enough to implement complicated trigger systems and stereo schemes which need more time to receive the trigger information from other telescopes. On the other hand, NECTAr is optimized to be cheap and reliable, so specific ASICs integrations have been used as much as possible. Thus, NECTAr front-end board uses specific Amplifiers for CTA (ACTA [98]) chips and also integrates the analog sampling memories and ADC converters in a single cheap, also dubbed NECTAr. Moreover, an integrated design of the pixel-level and camera-level trigger subsystems in two ASICs is under development with the aim to integrate all critical functions (see chapter 8).



(a) Dragon front-end board



(b) NECTAr front-end board

Figure 3.10: Dragon and NECTAr front-end boards

In order to develop the front-end boards and the trigger system in parallel, the trigger subsystems which will be housed in the front-end boards were developed in separated mezzanines, with the aim of integrating them in the front-end board for the production stage. Additionally working in this way has allowed us to test different trigger concepts with the same front-end boards, as well as testing the same trigger mezzanines in both Dragon and NECTAr front-end boards. In figure 3.10(a), in the upper side, the four connectors used for the mezzanine connection can be seen, while, in figure 3.10(b), the pixel-level and camera-level trigger mezzanines are connected.

3.2.1.3 Slow Control boards

The board known as slow control board³ (figure 3.11) provides the mechanical interface between the front-end board and the pixel electronics. Besides, it implements some slow control functions related with the high voltage control and DC anode current monitoring of the PMTs. It also contains temperature and humidity sensors which can be read by the FPGA in the front-end board. The slow control boards are different for LSTs and MSTs and have been developed by japanese and french groups respectively.

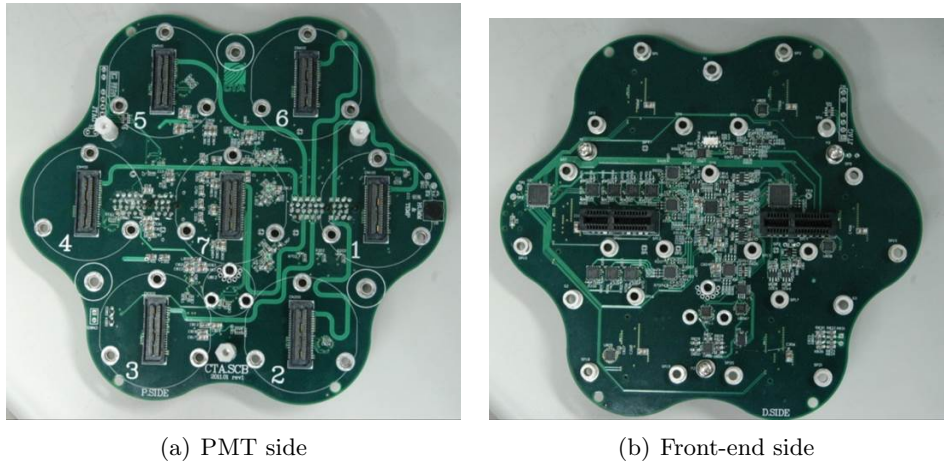


Figure 3.11: Slow control board

3.2.1.4 Backplanes

The backplanes (figure 3.12, manufactured by Ciemat group with some contribution from GAE-UCM and the author of this thesis) are connected to the front-end boards in the opposite side of the PMTs, being the mechanical interface between the high density connector of the front-end board and other camera subsystems, and implementing several functions. Two of this functions consist of providing connectivity with the camera power supply and the Ethernet switches for data and slow control communication. In these cases, every cluster has a cable dedicated only for each of these functions (star connection) to camera central systems. However, the main feature of the backplanes is that, in addition to be connected with the central systems, every backplane is connected to its six direct neighbours, forming a network which can be used to distribute signals. In this way, the backplanes are used to distribute clock, 1 PPS and different trigger signals throughout the camera. The way in which the signal distribution is implemented is described in depth in section 3.2.6, but it is obvious that this kind of distribution reduces drastically the amount of cables, and therefore their weight.

³It is interesting to remark that, paradoxically, the slow control board does not belong to the slow control system. It was named “slow control board” just because it controls the PMT high voltage.

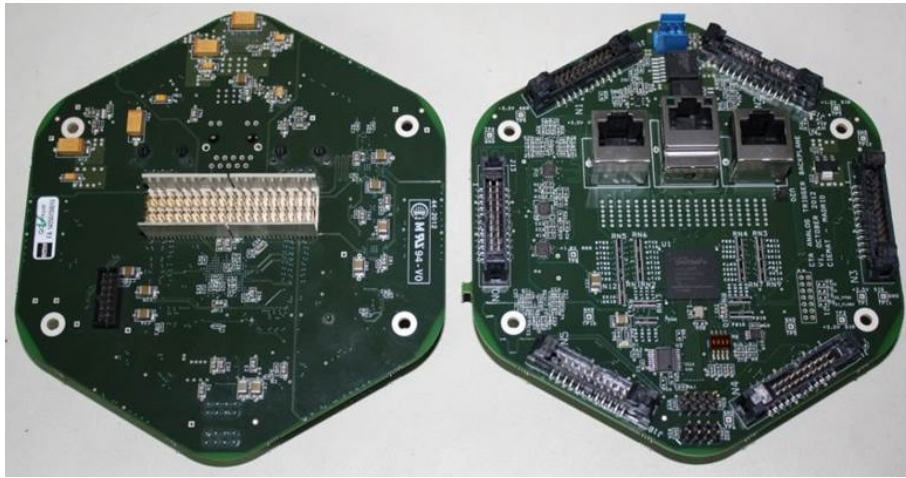


Figure 3.12: Backplane board

3.2.1.5 Trigger interface board

Once the trigger decision has been taken in the camera trigger, the trigger signal is sent to the central backplane and from here to the Trigger Interface Board (TIB) designed by the author of this thesis at GAE-UCM. This board (fig. 3.13) gathers different trigger origins, such as local level 1 triggers, calibration triggers, full CTA array triggers, etc. and produces the final trigger command which is send to the central backplane again to be distributed to all the clusters in order to actually start their readout. In the case of LSTs, the trigger interface board of each camera is also connected to the TIBs of the neighbour LSTs sharing their trigger information in order to implement stereo trigger schemes. This board is described in depth in chapter 7.



Figure 3.13: Trigger interface board